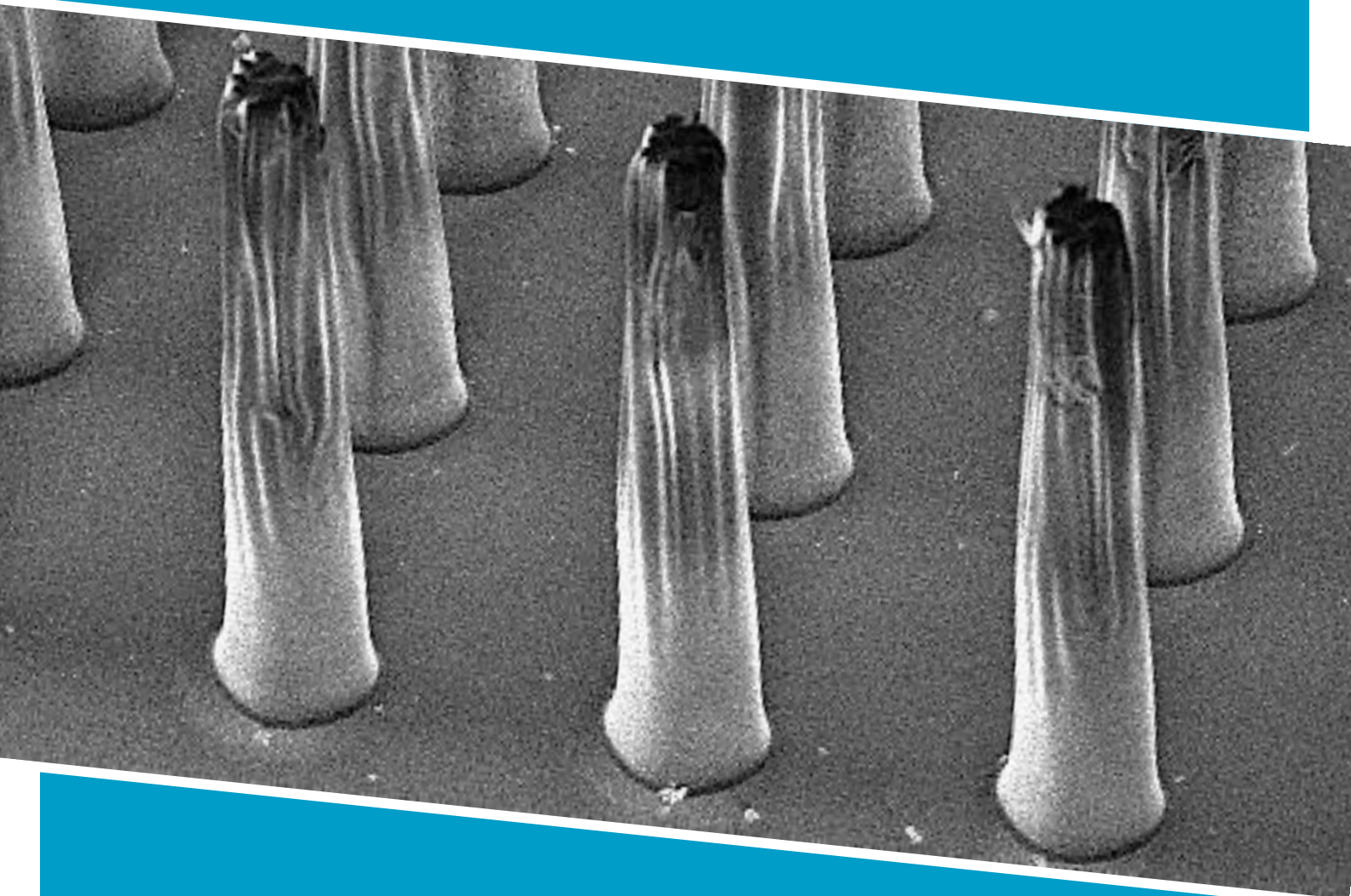


Microneedles for Optical Spectroscopy

**To measure across
the skin barrier**

E.S. Demirci



Microneedles for Optical Spectroscopy: To measure across the skin barrier

Microneedles for Optical Spectroscopy

To measure across the skin barrier

By

E.S. Demirci

In partial fulfilment of the requirements for the degree of

Master of Science
in Biomedical Engineering

at the Delft University of Technology,
to be defended publicly on December 16, 2019 at 9:00 AM.

Student number:	4529871
Project duration:	January 1, 2019 – November 25, 2019
Thesis committee:	Prof. dr. P.J. French EEMCS, ME, BE Dr. G. de Graaf EEMCS, ME, EI Dr. G. Pandraud EEMCS, ESE, PVMD

An electronic version of this thesis is available at: <https://repository.tudelft.nl/>

Background This project provides a proof of principle to use microneedles in combination with optical spectroscopy for bilirubin detection. For newborns, high bilirubin levels in the blood can lead to serious health consequences, such as jaundice, which can lead to brain damage. Therefore, it should be detected as early as possible. However, bilirubin monitoring of newborns in remote African areas is insufficient. In these areas the current invasive methods are time-consuming, and minimally invasive methods, such as bilirubinometers, are quite expensive, and may be inaccurate in babies with stronger skin pigmentation. In short, the conditions are not optimal to detect jaundice, and therefore an affordable method is needed to accurately and quickly measure the concentration of bilirubin. **Aim** The aim of this project was to develop microneedles for optical spectroscopy, and to test them in simulated skin to determine the usability for reflection measurements. **Fabrication** Microneedles are created by using microfabrication techniques with a focus on backside exposure. Multiple prototypes have been developed and evaluated based on dimensional properties. The prototype closest to the requirements was chosen to take measurements. These were the microneedles with an average length of 410 μm , an average base diameter of 106 μm and an average tip diameter of 43 μm . **Measurements** To test the microneedles for their performance, an indentation test, and transmission and reflection measurements has been performed. The indentation test showed that the average fracture point of one microneedle is at a force of 72.5 mN and an average displacement of 63 μm . The fracture point per area microneedle is on average 16.5 N/mm^2 . Furthermore, transmission measurements have shown that the reduction in transmission is 70 % from the base and 75 % from the tip. Therefore, the maximum amount of light that can be used for reflection measurements is 7.5 %. Moreover, reflection measurements have shown that the differences in color concentrations in the simulated skin results in differences in absorption and therefore reflection values. Also, the measurements in simulated bilirubin (skin simulation with yellow colorant) showed a dip in the blue spectrum, e.g. at 460 nm, the absorption peak of bilirubin. **Conclusion** In this project microneedles have been developed that are minimally invasive, biocompatible, optically transparent, and easy-to-process. The first measurements have shown that it seems possible to use the microneedles in combination with optical spectroscopy to detect differences in “bilirubin” concentrations. Moreover, the microneedles can be used to puncture the skin without fracturing. However, the actual usability in the clinical setting still needs to be investigated. Other important recommendations for future research are research into measurements with real bilirubin; the optimal alignment between the microneedles and the optical spectrometer; optimization in the manufacturing process to cover the spaces between the microneedles; and possible other development methods for microneedles (e.g. 3D printing) and other designs (e.g. mirrors for efficient light use).

Contents

1 Introduction	3
1-1 Problem and relevance	3
1-2 Possible solution and aim	4
1-3 Thesis structure	4
2 The skin.....	5
2-1 Skin histology.....	5
2-2 Absorption and scattering in the skin	6
2-3 Skin resistance	10
3 Measurement methods for bilirubin.....	11
3-1 Current measurement methods	11
3-2 Measurement methods in recent literature	12
3-3 Our solution	13
4 Microneedle design	14
4-1 Microneedle types	14
4-2 General microneedle design considerations.....	14
4-3 Microneedle design requirements.....	15
5 Microneedle fabrication.....	17
5-1 Common microneedle fabrication method.....	17
5-2 Fabrication process.....	17
5-3 Fabrication results	21
6 Measurements	24
6-1 Dimensional aspects	24
6-2 Mechanical failure	24
6-3 Transmission	26
6-4 Reflection.....	30
7 Conclusion and future work	33
References	35
Appendix	38

Microneedles for Optical Spectroscopy: To measure across the skin barrier

1 Introduction

This report describes the design and fabrication of microneedles for optical spectroscopy in simulated human tissue. The project is focused on the detection of bilirubin in blood using a low-cost minimally invasive system, although there may be many more applications for the fabricated microneedles.

1-1 Problem and relevance

According to field research by Stellenbosch University in South Africa, there are no suitable methods to measure bilirubin in newborns in remote African areas, and this can have serious consequences. Bilirubin is a yellow, toxic product which is released by degradation of hemoglobin in red blood cells. Because bilirubin is not water soluble, it is transferred through the bloodstream bound to the plasma protein albumin. In this form, it is known as conjugated bilirubin, which is then further metabolized and excreted via the faeces [1]. Very high levels of bilirubin, called hyperbilirubinemia, lead to jaundice, which is a yellow discoloration of the eyes and skin caused by excessive bilirubin in the skin and mucous membranes. In neonatal jaundice there is an imbalance between bilirubin production and conjugation, which leads to increased bilirubin levels. This imbalance is mainly caused by the immature liver of the neonate and the fast breakdown of red blood cells. Approximately 60 % of the full-term babies and 80 % of the premature babies experience hyperbilirubinemia. The average neonatal jaundice is often not life threatening. However, in case of severe jaundice, bilirubin accumulates in the brain and provoke kernicterus, which can result in irreversible brain damage, cerebral palsy and hearing impairment [2-4]. Therefore, it is important to diagnose bilirubin levels in high-risk population groups, such as newborns, and manage it appropriately. Ideally, the bilirubin level of all babies should be checked at birth and again three days after birth [1].

As previously indicated, bilirubin monitoring of newborns in remote African areas is insufficient. There are several reasons for this. Firstly, in these areas the current invasive method for measuring bilirubin by taking a blood sample is time-consuming since there are no facilities nearby where the blood sample can be examined. Moreover, taking a blood sample is invasive, can be painful, and has a higher risk of infection on the sampling site. Furthermore, noninvasive methods, such as bilirubinometers (i.e. Philips BiliChek and JM-103 bilirubinometer), a method based on the principle of multi wavelength spectral reflectance of bilirubin staining in the skin, are quite expensive [5]. Besides that, these bilirubinometers may overestimate the bilirubin concentration in colored babies caused by the stronger skin pigmentation and are therefore inaccurate for this group [6]. This may result in unnecessary treatment, which is a burden for the patient and a waste of money, especially in poor remote African areas. Also, there are few to no qualified people in these areas who can perform bilirubin measurements. In short, the conditions in remote African areas are not suitable to detect hyperbilirubinemia. For these areas, an affordable and a non- or minimally invasive method is needed to easily, accurately and quickly measure the concentration of bilirubin, especially in resource-limited settings.

1-2 Possible solution and aim

Optical spectroscopy, the measurement of optical properties of a biospecimen by following light interactions with the specimen, is one of the methods used in biosensors [7]. This is also a method that is used in bilirubinometers, but which is negatively influenced by the amount of pigmentation [6]. More pigmentation results in more absorption of light, and therefore less reflection. To minimize the effect of pigmentation, the use of optical spectroscopy just below the skin layer that contains the pigmentation could be a solution. However, this construction requires a device that transports light through the skin. A study by Kwon et al. [8] shows that this is possible by using microneedles as 'waveguides'. A big advantage of microneedles is that, compared to conventional needles, they have a smaller risk of infection and produce little to no pain sensation. This is because microneedles hardly have any interactions with the innermost layer of the skin, the dermis, where sensory nerve endings are located [9]. Kwon et al. [8] have developed microneedles for the optical stimulation of cortical neurons in specific brain areas with a light emitting diode (LED). However, this is only a part of optical spectroscopy, namely the 'input' of light into the human body. In optical spectroscopy there is also an 'output' of light, which is an important variable when measuring bilirubin, as it indicates its amount. Therefore, the aim of this project was to develop microneedles for optical spectroscopy, and to test them in simulated skin to determine the usability for reflection measurements.

1-3 Thesis structure

[Chapter 2](#) describes background information about the skin, its structure, optical and mechanical properties. [Chapter 3](#) provides information about current methodologies for measuring bilirubin followed by an overview of the solution provided by this project. [Chapter 4](#) starts with literature on microneedle types and design considerations when developing microneedles. Subsequently, the design requirements and the design of the microneedles of this project are discussed. [Chapter 5](#) starts with literature on the general methodology to fabricate microneedles and presents the complete process for producing the microneedles with the corresponding results. [Chapter 6](#) shows measurements of dimensional aspects, mechanical failure and optical properties of the microneedles focused on transmission and reflection. [Chapter 7](#) concludes this report and contains recommendations for future research.

2 The skin

2-1 Skin histology

The skin is an organized structure consisting of three major layers, called the epidermis, dermis, and hypodermis. The epidermis is the outermost layer and has a thickness of approximately 75-150 μm , depending on the location. The epidermis consists of four to five sublayers, from outermost to innermost called stratum corneum, stratum lucidum (only in soles and palms), stratum granulosum, stratum spinosum, and stratum basale (Figure 1). The epidermis consists of a variety of cell types, for example, keratinocytes which produce keratin which serves as a protective overcoat, and melanocytes, cells responsible for producing melanin that gives colour to the skin and protects it from ultraviolet radiation. The dermis, the layer between the epidermis and the hypodermis, is a thick layer which contains connective tissue, such as collagen and elastin, which dictates the mechanical behaviour of the skin. Furthermore, the dermis contains nerve endings, blood vessels, hair shafts, and sweat glands. The epidermis and dermis together have a thickness of approximately 1.5-2.5 mm. The innermost layer, the hypodermis, consists mainly of adipose tissue (fat cells) [10-11].

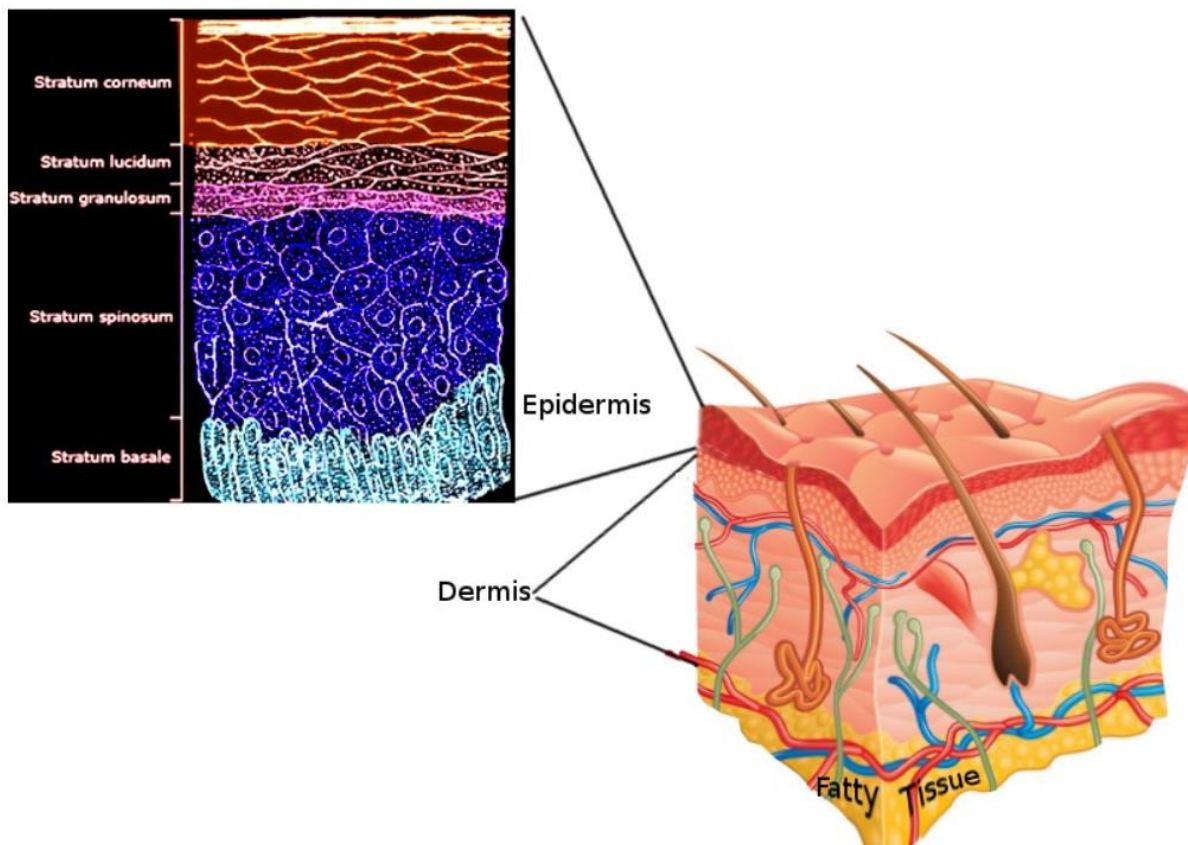


Figure 1 – Schematic view of the human skin

2-2 Absorption and scattering in the skin

The optical properties of the skin must be considered when measuring bilirubin with optical spectroscopy, so that the measurements are interpreted correctly. Optical properties of the skin depend on the location and histology of the skin layers. Light that meets the skin surface can be reflected to the environment or transmitted to deeper layers. Light that penetrates the deeper layers can be attenuated. Attenuation is the process by which photons are 'removed' from a light beam while propagating through a matter where absorption and scattering occurs. Eventually, some of the light can be propagated back to the environment.

Absorption of light means that light is converted into energy. If the electromagnetic frequency of the light corresponds to the electromagnetic frequency of the matter, the light will be absorbed, and otherwise it is transmitted or reflected. Scattering means that light is converted into energy and that the energy is re-emitted as light in different directions. Scattering is a form of reflection where there is diffuse reflection where light is 'lost' and non-scattering reflection, called specular reflection, can be captured by a sensor. Thus, attenuation of light can be caused by absorption and scattering. The attenuation depends on the thickness of the matter through which the light travels. The attenuation coefficient indicates the amount of attenuation and is therefore the sum of the absorption coefficient and the scattering coefficient. The attenuation coefficient is inversely proportional related to the average distance that photons can travel before they interact [12]. Thus, if the attenuation coefficient increases, the travel distance of the photons decreases.

Figure 2 shows where scattering and absorption take place in the skin layers. This takes place in both the epidermis and the dermis (the hypodermis is not shown here). However, different substances lead to absorption and scattering, which differs per skin layer.

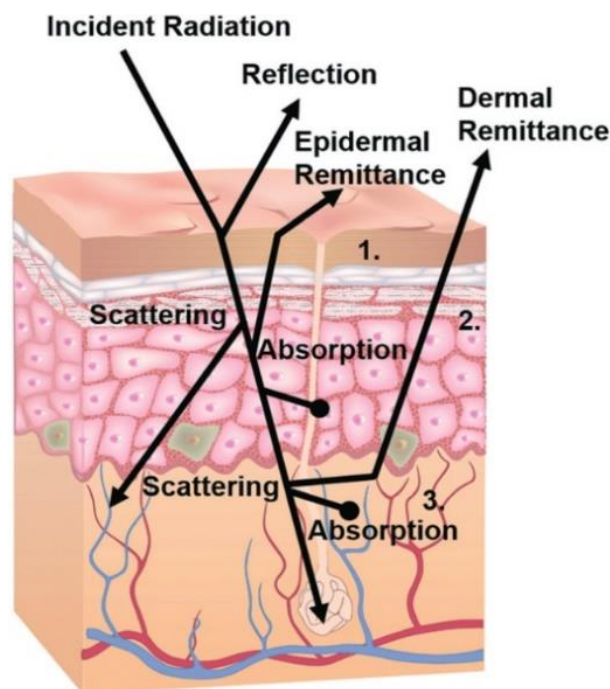


Figure 2 – Schematic view of optical pathways in skin (1 = keratin, 2 = melanin, 3 = hemoglobin and bilirubin)

The amount of absorption and scattering differ between skin layers. Figure 3 shows the absorption (A) and scattering coefficients (B) of the epidermis and the dermis of Caucasian subjects. At 460 nm, the absorption coefficients in the epidermis and dermis are 0.09 and 0.06 cm^{-1} respectively. At 460 nm, the scattering coefficients in the epidermis and dermis are 0.85 and 0.55 cm^{-1} respectively [13].

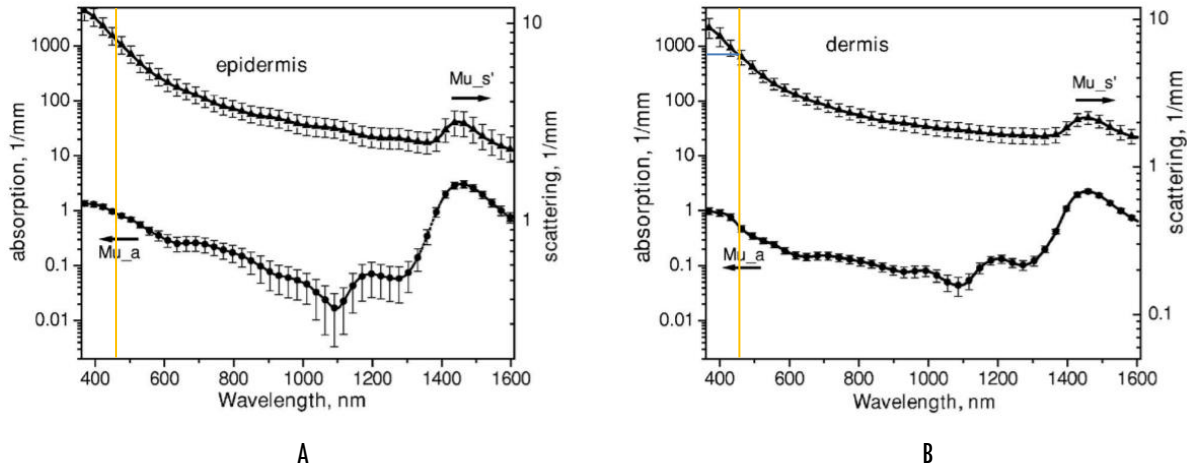


Figure 3 – Absorption (circles) and scattering (triangles) coefficients of the epidermis and dermis

Figure 4 shows the absorption coefficients of the main components in the skin. In the epidermis, melanin mainly causes absorption. Melanin plays a major role in absorption in the visible domain. Moreover, blood (hemoglobin) and yellow pigments (bilirubin) mainly cause absorption in the dermis. Hemoglobin and bilirubin absorb also in the visible domain. The graph shows that the absorption coefficient of hemoglobin and bilirubin is approximately the same. Furthermore, in the hypodermis, fat mainly causes absorption, with a high absorption in the infrared domain. Lastly, water plays a role in all skin layers and has a high absorption in the infrared domain [14].

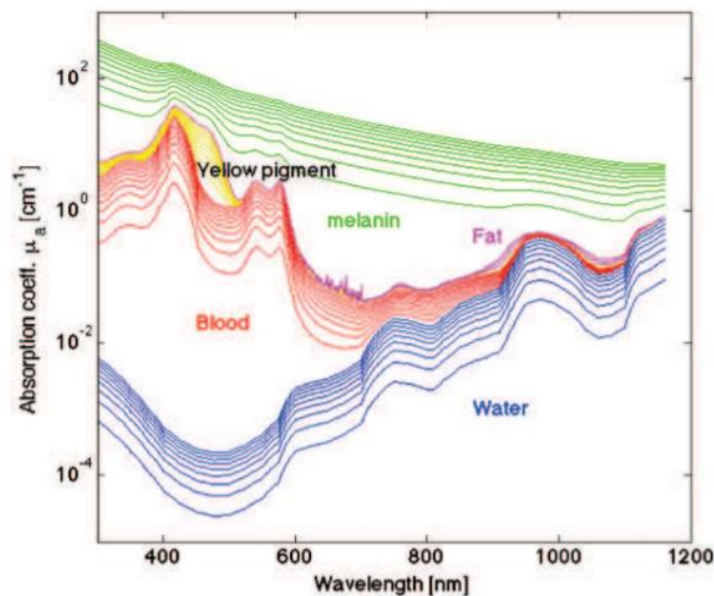


Figure 4 – Absorption coefficients of the main components in tissue

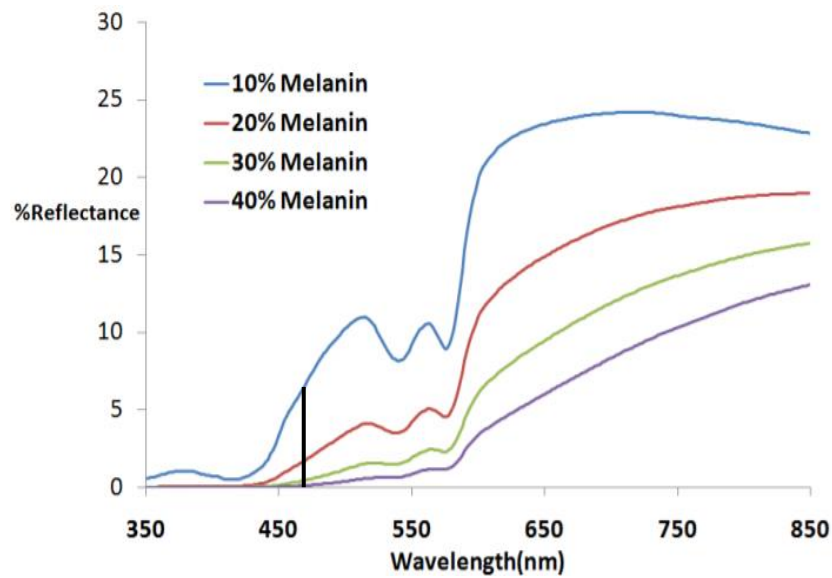


Figure 5 – Reflectance spectra of human skin for varying melanin concentration

The epidermis, specifically the stratum basale, contains a lot of melanin. The amount of melanin in the skin has a significant influence on bilirubin measurements with optical spectroscopy. Figure 5 shows that a higher melanin concentration in the epidermis results in more absorption by melanin, and therefore less reflection in the wavelength region of bilirubin [15]. Thus, this layer will have to be eliminated with bilirubin measurements.

In healthy individuals, bilirubin is present in a small amount. However, in persons whose liver functions do not work properly or with a large amount of red blood cell breakdown, the bilirubin amount is higher. This increases the absorption of light by bilirubin. Research has shown that bilirubin has a peak absorption at 460 nm (Table 1). A higher bilirubin concentration results in more absorption by bilirubin, and therefore less reflection in the wavelength region of bilirubin (Figure 6) [15].

Article	Absorption spectrum (nm)
Javid et al. [16]	457-473, peak at 460
Lodha et al. [17]	440-530, peak at 460
Mohamad et al. [18]	400-600
Sudha et al. [19]	460-550
Veenstra et al. [20]	440-660, peak at 460

Table 1 – Absorption spectrum of bilirubin

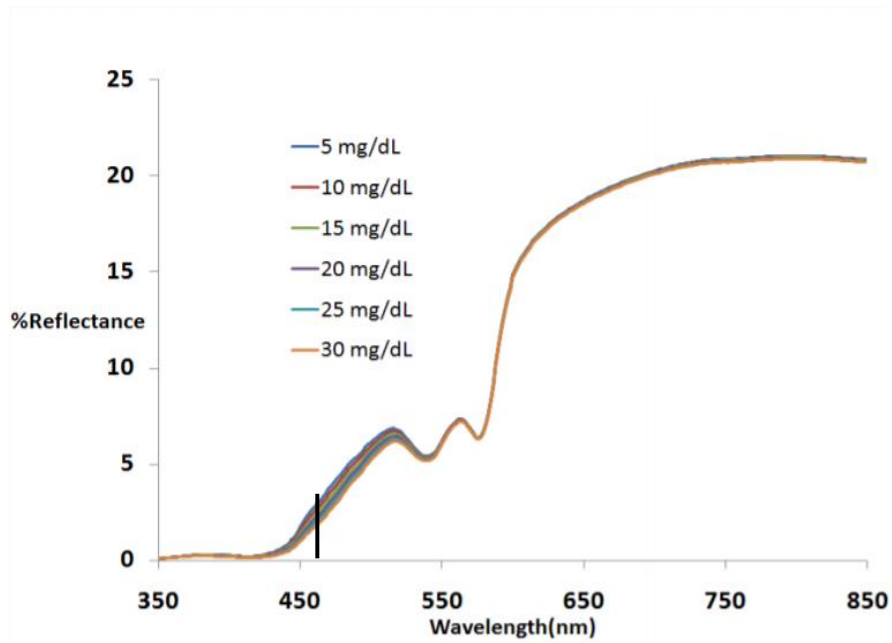


Figure 6 – Reflection at different concentrations of bilirubin

When measuring the amount of bilirubin with optical spectroscopy, substances that absorb in a comparable wavelength range must be considered. As mentioned above, the absorption wavelength spectra of haemoglobin partly overlap with that of bilirubin. This is also shown in Figure 7. Overlapping spectra can influence the accuracy of the measurements [21].

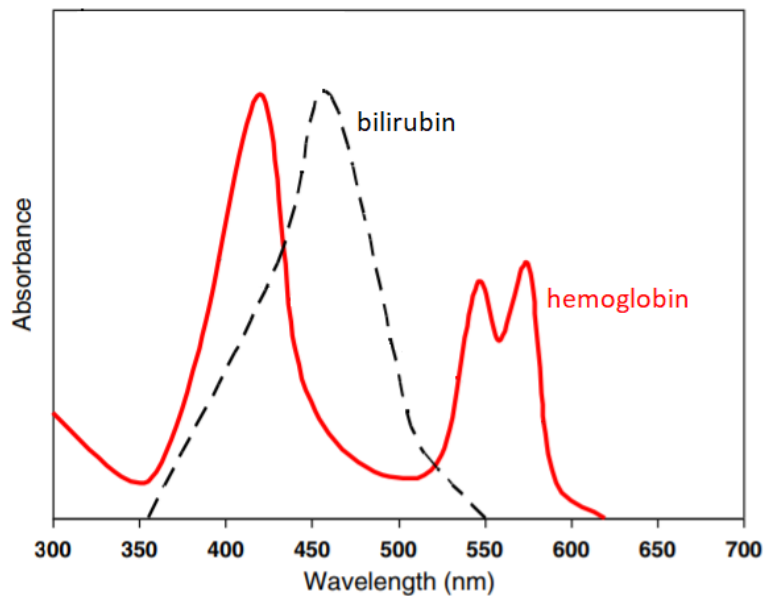


Figure 7 – Absorption spectrum of bilirubin and hemoglobin

As indicated above, scattering also influences the attenuation of light. Scattering in the skin is mainly caused by proteins. Keratin, filamentous protein, plays a major role in light scattering in the epidermis. In addition, melanin contributes significantly to the amount of scattering in the epidermis. However, the amount of scattering caused by melanin varies substantially between individuals, because the volume fraction, distribution and size of melanin varies between skin types. In the dermis, collagen causes scattering [22].

Conclusion

Melanin play a major role in absorption of light in the skin. This concerns the outermost layer of the skin, the epidermis. Especially in people with a higher amount of melanin in the skin, a lot of light is absorbed in the visible domain. In addition to absorption in the epidermis, the amount of scattering in this layer is also high relative to the dermis. This is also caused by melanin, but also by keratin. Thus, both the absorption and the scattering are high in the epidermis compared to the dermis. Therefore, when measuring substances, such as bilirubin, in the dermis with optical spectroscopy it is desirable to eliminate the epidermis. Furthermore, hemoglobin in the dermis influences the reflectance spectra in the visible domain. Therefore, in the case of bilirubin measurements, it is important to consider the interference by hemoglobin.

2-3 Skin resistance

The mechanical properties of the skin play a role in, for example, puncturing the skin. When puncturing the skin, the needle will experience resistive forces exerted by the skin. In order to puncture the skin, the ultimate stress of the skin must be overcome by pushing perpendicular to the skin with the needle to bend and stretch the skin. In addition, other factors also play a role in stretching the skin, such as the stiffness of the tissue underneath. Several mechanical properties of the skin can be found in the literature. However, there is a wide range of variation in the numbers, because the mechanical properties depend on factors such as the hydration of the skin, age, location on the body and the testing method, and these are not always clearly stated.

According to Jacquemoud et al. [23], the ultimate stress of human skin is 3.0 N/mm^2 . Furthermore, the Young's modulus (stiffness) of the overall epidermis is 1.1 N/mm^2 , and the Young's modulus of the dermis is approximately 7.3 N/mm^2 [24]. Thus, the dermis is stiffer compared to the epidermis. Moreover, aging influences the mechanical properties of the skin. The stiffness of the skin increases linearly during aging, and aging also makes the skin thinner, less tense and less flexible. For example, the thickness of the epidermis and the dermis together is $0.7 - 0.8 \text{ mm}$ smaller in elderly people compared to normal skin [23].

According to Aggarwal et al. [25], the theoretical force required to puncture the skin (F_{puncture}) is 3.2 N/mm^2 , which is slightly higher than stated by Jacquemoud et al. [23]. Once the skin is punctured, this force is much lower. Moreover, the tip diameter of the needle plays a role in the ease of puncturing the skin. If the tip diameter is very small, the load on the needle becomes more concentrated during puncturing. As a result, the ultimate stress will be reached faster.

3 Measurement methods for bilirubin

3-1 Current measurement methods

The concentration of bilirubin in the human body can be detected through several techniques, which can be subdivided into two categories: invasive and non-invasive. In invasive detection methods blood is taken, commonly performed by a heel stick, for laboratory testing of the blood sample. Currently, this is the gold standard to measure the concentration of bilirubin. It is the most used method worldwide, because it accurately measures the concentration of bilirubin. However, taking a blood sample may lead to unnecessary blood loss, pain, stress, and an increased risk for infection at the sampling site [20]. In non-invasive detection methods, a blood sample is not necessary. The most obvious example of a non-invasive method is the use of the human eyes to look at the yellow discoloration of the skin. This is a cheap technique and easy to implement. However, knowledge about the condition and symptoms is needed. After detection with the eye, a check via a blood sample is still required to record the amount of bilirubin. Moreover, optical spectroscopy is used to measure the concentration of bilirubin. There are bilirubinometers on the market that measure the concentration of bilirubin by means of optical spectrometry, such as the Philips BiliChek (Figure 1) and the JM-103 bilirubinometer.

The Philips BiliChek measures bilirubin by using white light. The device directs the light through a disposable tip into the skin of the forehead or the sternum and measures the intensity of the wavelengths that return. The amount of bilirubin is determined by considering the spectral properties of hemoglobin and melanin. Philips indicates that the BiliChek can be used with all variations in skin tone [26]. However, according to the research of Olusanya et al. [3], the device overestimates the amount of bilirubin in neonates with more pigmentation.



Figure 1 – Philips BiliChek

3-2 Measurement methods in recent literature

In addition to the existing methods for measuring bilirubin, research is being done into other methods. In recent literature, the focus is on minimally invasive devices. The most common method in recent literature is the use of a smartphone camera in combination with an application and a color calibration card (Figure 2). With this method a photo is made of the color card on the baby's skin. The application on the smartphone (i.e. BiliCam and BiliScan) determines the yellowness of the skin using image processing techniques and relates this to a certain bilirubin concentration. This method is cheap, easy to implement, and the processing time is short. However, all studies show that the accuracy is not yet optimal [27-29].



Figure 2 – Smartphone camera with color calibration card

Furthermore, the combination of a dermatoscope, a magnifying loupe with a built-in light source, with a smartphone camera and image processing techniques to determine the yellowness of the skin was investigated (Figure 3). The authors indicate that this is an easy to implement method. However, according to the authors, a dermatoscope is difficult to obtain and has a low level of validity for clinical use [30]. Lastly, there are several studies in which optical spectroscopy is used in another way to measure the concentration of bilirubin. However, all studies indicate that the accuracy is not optimal. [20, 30-31].



Figure 3 – Smartphone camera with dermatoscope

3-3 Our solution

As described above, taking a blood sample is the gold standard to measure the concentration of bilirubin. However, this is an invasive method, causes pain and increases the risk of infection. A widely used minimally invasive method is a bilirubinometer, which is easy to use and reliable. However, it is not accurate enough in babies with high pigmentation levels. It is also too expensive for many remote areas. For these reasons, our proposal is to develop a method where optical spectrometry is used to measure the amount of bilirubin, but in which the effect of pigments is eliminated as much as possible. This mainly concerns the epidermis. In addition, the proposed solution is expected to be minimally invasive, accurate, inexpensive, quick and easy to use by unqualified persons. Figure 4 shows schematically our idea. The device consists of an optical spectrometer connected by a fiber to microneedles that puncture the skin. The microneedles, built on a transparent substrate, act as a ‘tunnel’ to get light in and out of the skin. The optical spectrometer is a fixed device, and therefore only needs to be purchased once. The microneedles are made from an optically transparent, inexpensive, easy-to-process and biocompatible material, and are disposable.

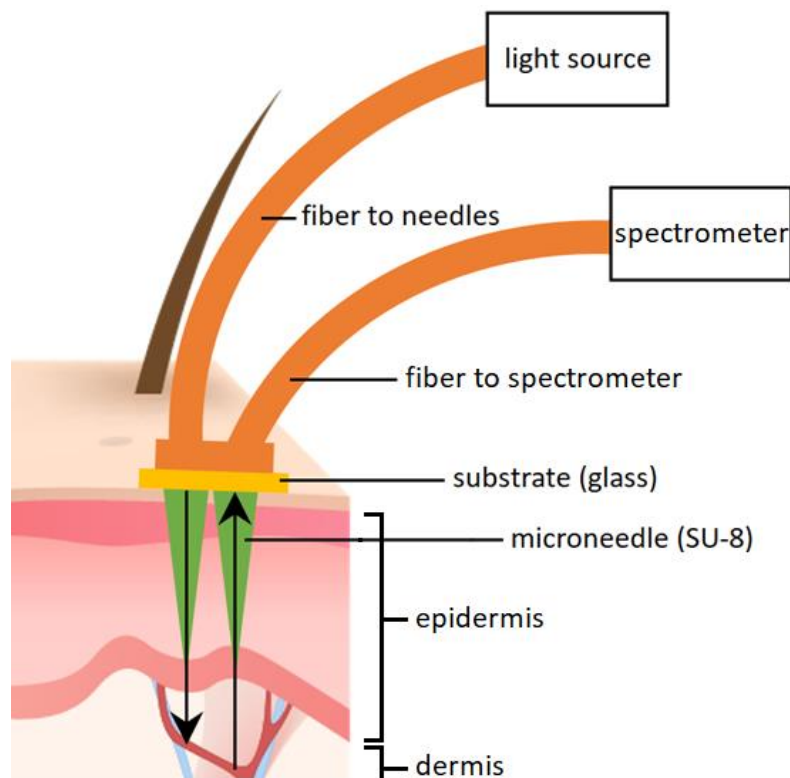


Figure 4 – Schematic view of our solution

4 Microneedle design

4-1 Microneedle types

Microneedles can be roughly divided into two types: microneedles for therapeutics and microneedles for diagnostics. In therapeutics, microneedles can be categorized into four subtypes: solid, hollow, coated and dissolving (Figure 1). Solid microneedles are solidified with micron sized pores, allowing slow diffusion of compounds. Hollow microneedles allow the diffusion of compounds through a lumen, comparable with conventional infusion needles. Coated microneedles are coated with dissolvable compounds. Dissolving microneedles are biodegradable and encapsulated with compounds, which dissolves completely when inserted into the skin [9]. In diagnostics and monitoring applications, microneedles can be categorized into four subtypes: microneedles for interstitial fluid sampling, for selective “catching” of biomarkers, for biomarker monitoring, and for biopotential measurements (Figure 2) [33]. Most of the publications in diagnostic and monitoring applications involve microneedles used for monitoring of glucose levels in the interstitial fluid [34-36]. They are also applied in the detection of lactate [37], cholesterol [37], pH [39], protein [40], cancer [41], and alcohol [42].

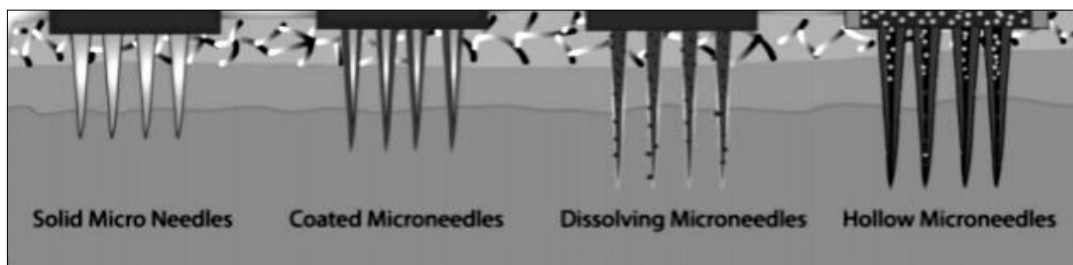


Figure 1 – Microneedle types in therapeutics

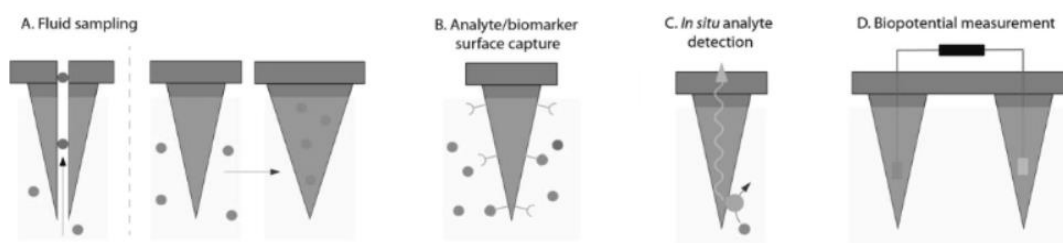


Figure 2 – Microneedle types in diagnostics

4-2 General microneedle design considerations

Several articles have highlighted several design considerations that have to be considered when designing microneedles [43]. Starting with the geometrical aspects that need to be considered, the length of the microneedles is an important aspect. The length of the microneedles must be long enough to puncture the stratum corneum and short enough not to reach the dermis, where nerve endings are located, such as for pain, pressure and temperature. In this way, the use of microneedles will be pain-free and minimally invasive. The tip sharpness is also involved in this. The sharper the tip,

the easier it is to puncture through the skin. Furthermore, the choice for the shape and type of the microneedles is also important and depends on the purpose for which it will be used. For example, if a substance must be extracted from the body, a hollow type must be chosen. In contrast, a solid type is useful when signals need to be measured. The tip radius is dependent on the choice of the type; the hollow type usually has a larger tip radius compared to a solid type. In addition to the geometrical aspects, the mechanical aspects of the microneedles must be examined. It is crucial that the microneedles do not break when puncturing into the skin. To successfully penetrate the skin and to keep the risk of fracture as low as possible, the microneedles need to be designed mechanically stronger/tougher than the skin. Mechanically, skin is a heterogeneous, anisotropic, and non-linear viscoelastic material. The effectiveness of microneedles used in biosensors is dependent on an efficient and stable insertion of the microneedles into the skin at a specific depth. In order to achieve this successfully, the mechanical insertion of the microneedles should be 'matched' to the mechanical properties of the human skin, which are primarily the Young's modulus and the skin breaking stress/ultimate stress [44]. Other design considerations that can be looked at are related to the manufacturing process. First, if there is a limited budget, it is essential to take the costs of the manufacturing procedures into account. The choice of materials plays a role here. For example, micromachining processes used to develop microneedles usually requires a cleanroom, which increases the costs. Besides that, if the product must be produced cheaply on a large scale, then the scalability of the manufacturing process on a commercial scale is important to think about. Lastly, an important design requirement in medical applications is biocompatibility, the ability of the microneedles (used materials) to function without generating an immune response. To avoid infections, the possibility to sterilize the microneedles before use is also desirable. Based on the guidelines of the United States Food and Drug Administration, the endotoxin content should be lower than 20 EU per device. There is a possibility to design a device fully aseptic, but this could increase the manufacturing costs.

4-3 Microneedle design requirements

The microneedles to measure bilirubin optically must meet the following requirements:

1. It must be biocompatible;

The microneedles will enter the skin and should therefore not cause any unwanted reactions.

2. It must be able to pierce the skin;

The tip of the microneedles must have enough surface for passing light and must be sharp enough to pierce the skin. Kwon et al. have shown that tips with a smaller diameter allow less light to pass through compared to tips with a larger diameter. For example, no light passes through a tip with a diameter of 10 μm . A tip diameter of 30, 40 and 50 μm gives a light flux of 20, 30 and 45 % respectively [8]. The diameter of the tip must be as large as possible, but also sharp enough to pierce the skin. A tip diameter of approximately 40 μm has been chosen for this project.

3. It must provide enough mechanical strength for insertion into the skin;

It is important that the tip of the needles do not break and that the overall structure has the required mechanical strength to withstand the force applied during insertion into the skin. The theoretical force required to puncture the skin (F_{puncture}) is 3.2 N/mm^2 [25].

4. It must be minimally invasive;

The length of the microneedles must be long enough to puncture the dermis, and short enough to avoid contact with the sensory nerve endings. The skin thickness depends on the location. Because it is not yet known which location for bilirubin measurements is the most ideal, the length of the microneedles is based on the study by Gill et al. According to that research, a microneedle with a length of 480 μm only gives 5 % of the pain of a conventional needle. The longer the microneedle, the more pain is experienced. In addition, the number of microneedles also influences pain, as more sensory nerves are stimulated. The use of five microneedles accounted for 10 % of the pain of a conventional needle [45]. Based on this information, a length of 400 μm has been chosen. With this length, the dermis is punctured well, and the pain will be minimal.

5. It must be optically transparent for the wavelengths of bilirubin;

SU-8 is an epoxy-based negative photoresist which is transparent for the wavelengths of bilirubin, biocompatible, cheap to process, and suitable for high aspect ratio structures [46].

6. It must be accurate and reliable in clinical application;
7. It must be easy to integrate with a spectrometer;
8. It must be cheap to produce;
9. It must be easy to use (by people without qualifications).

In this project the focus was on requirements 1 to 5. Three approaches to meet these requirements have been developed through co-creation. The approaches differ in the design of the tip, with the focus on efficient use of light. The first approach focuses on developing microneedles from SU-8 only (Figure 3A). The processing steps can be found in the next chapter and in [Appendix A1](#). With the second and third approaches, the focus is more on the (expected) efficient use of light. In the second approach, there is a convex 'mirror' of metal in the tip of the microneedle. The expectation is that more light will go in and out of the microneedle as a result (Figure 3B). However, more processing steps are required to create this type of microneedle. The third approach is like the second approach; however, it contains 'mirrors' in the form of nanoparticles (for example, gold) instead of a convex one (Figure 3C). A possible processing flowchart of the second design approach can be found in [Appendix A2](#). In this project it was decided to implement the first approach, because of the time available for this project and the options available (i.e. equipment and expertise) in the relevant cleanroom.

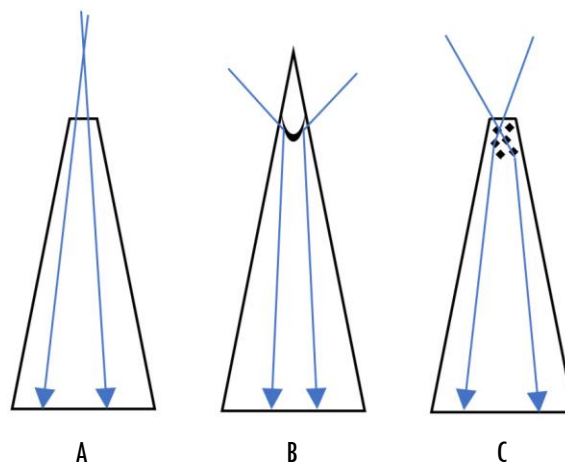


Figure 3 – Design approaches (schematic)

5 Microneedle fabrication

5-1 Common microneedle fabrication method

Microneedles have been manufactured from various materials (e.g., metal, polymers and silicon) with different lengths, features, and shapes (e.g., canonical, cylindrical and pyramidal). Microelectromechanical systems (MEMS) technology is the most common method for developing microneedles, because it allows the production of very small structures and very precise devices. Most fabrication methods for microneedles are based on microfabrication techniques, such as adding, removing, and copying microstructures by making use of photolithographic processes, laser cutting, metal electroplating, silicon etching, metal electropolishing and micromoulding.

Generally, the manufacturing methods used for producing microneedles can be reduced to three basic techniques: deposition of thin films of the material on a substrate; applying a patterned mask on top of a film by photolithographic imaging; and etching the films carefully to the mask. Thin film deposition includes processing above the substrate surface (mostly silicon), in which the material is added to the substrate in the form of thin film layers. Deposition can be chemical, in which the material is deposited on the substrate through a chemical reaction, or physical, in which the material is physically moved onto the substrate surface. Subsequently, the film layers are patterned using photolithography to make copies of a pattern onto the surface of a substrate of the material. Finally, parts of the surface are etched away to release the final structure. This can be achieved by wet etching or dry etching. In wet etching, parts are removed by immersion in a liquid bath of a chemical etchant. In dry etching, parts are removed by exposing the parts to an attack of ions [47-48]. Microneedles are often provided with a coating at the end of the manufacturing process. In most cases in diagnostic and monitoring applications, microneedles function as electrodes. This sensing method for microneedles is usually chosen when it comes to detecting biosignals, such as in electroencephalography (EEG) and electromyography (EMG). Also, these are all solid microneedles. The mainly used materials are polymers (SU-8, PET, parylene, epoxy, PMMA, and PLA). Furthermore, gold (Au) is often used as a coating, and titanium (Ti) also seems to be a popular choice.

5-2 Fabrication process

The microneedles are manufactured by backside exposure. This process is based on the process described by Liqun et al. [49], and information from the datasheet for SU-8 [46]. The microneedles are built on a glass wafer ($\varnothing = 100$ mm, $t = 525$ μm), because of the transparency. The polymer SU-8 2075 (MicroChem Inc.) was used for the microneedles, since this variant of SU-8 has a high viscosity (more than 73 % solids) which is necessary to create thick layers onto the substrate. Eight prototypes have been made to optimize the parameters to obtain the desired microneedles. The parameters used in these prototypes are shown in Table 1. Prototype 4 was the closest to the desired microneedles. Below is the process shown to develop the desired microneedles. More schematic process steps can be found in [Appendix A1](#).

	#1	#2	#3	#4	#5	#6	#7	#8
Spin-coat	4×100	4×100	2×200	2×200	2×200	2×200	1×400	1×400
Soft bake at 65 °C (min.)	0	0	2×10	2×10	2×10	2×10	1×20	1×20
Soft bake at 95 °C (min.)	4×20	4×20	2×60	2×60	2×60	2×60	1×120	1×150
Exposure energy (mJ/cm ²)	1500	1500	2500	1750	1000	800	1750	1750
Proximity (μm)	60	60	130	130	130	130	130	130
Post-exposure bake at 65 °C (min.)	0	0	0	0	0	10	10	10
Post-exposure bake at 95 °C (min.)	15	15	20	20	20	20	20	20
Development (min.)	40	40	100	100	100	100	100	100
Spinning during development (rpm)	250	250	0	0	0	0	0	0
Drying with centrifuge	yes	no						

Table 1 – Prototypes with processing parameters

Step 0: Prepare

SU-8 is a very viscous material. To be able to use SU-8 more easily during processing, approximately 30 mL from the original bottle from the fridge was poured into a cup that was kept at cleanroom temperature in a room with yellow light (because of the cross-linking behavior of SU-8) for at least four hours before use.

Step 1: Spin-coat

The Brewer Science Manual Spinner is used to cover the wafer with the desired film thickness of SU-8. First, the wafer is centered and vacuumed on a contaminated chuck. Then approximately 10 mL SU-8 was directly poured from the cup at the center of the wafer (Figure 1). Subsequently the spinning started at a spinning speed of 500 rpm with an acceleration of 100 rpm per second and a spinning time of 5 s to spread the SU-8 a bit, following a spinning with a spinning at a speed of 1300 rpm with an acceleration of 300 rpm per second and a spinning time of 30 s to get a film thickness of 200 μm (Figure 2). After a rest of 5 minutes, the edge and the back of the wafer (still vacuumed to the chuck) were manually cleaned with a swab soaked in acetone.



Figure 1 – A drop of SU-8 at the center of the wafer

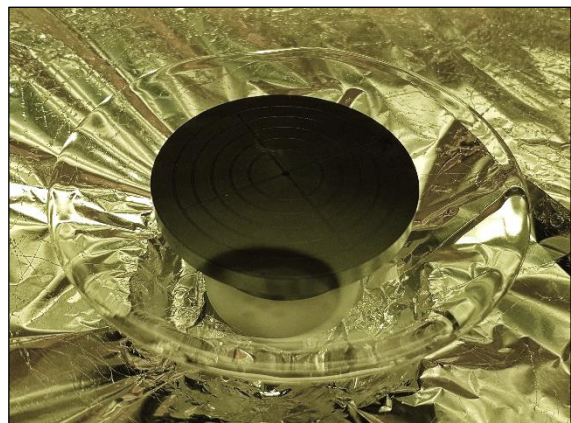


Figure 2 – Wafer coated with a layer of SU-8

Step 2: Soft bake

A mobile hotplate is used to soft bake the film (Figure 3). First, the film was baked for 10 minutes at 65 °C and then for 60 minutes at 95 °C. Subsequently, the wafer was removed from the hotplate and cooled for 10 minutes at cleanroom temperature.



Figure 3 – Soft baking SU-8 on mobile hotplate

Step 3: Spin-coat

Step 1 was repeated to achieve a thickness of 400 μm by creating a second film of 200 μm on the first film. The film layer is spun in two parts because it leads to more uniformity. If the layer is spun on it in one go, a "donut" is created in which the edge is thicker than the center.

Step 4: Soft bake

A mobile hotplate is used to soft bake the final film. First, the film was baked for 10 minutes at 65 °C and then for 60 minutes at 95 °C. Subsequently, the wafer was removed from the hotplate and cooled for 20 minutes at cleanroom temperature. Figure 4 shows the result.

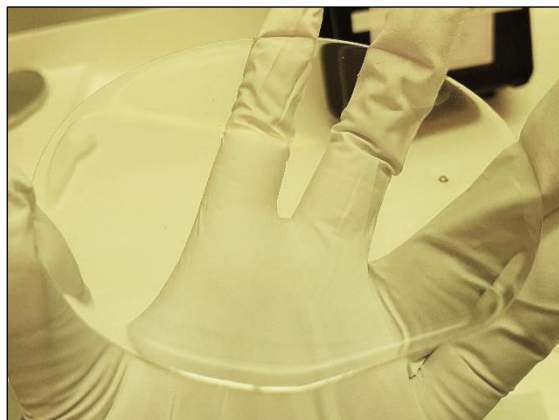


Figure 4 – Wafer coated with SU-8

Step 5: Exposure

The EVG420 Contact Aligner (with 465 nm (i-line), 405 nm (h-line), and 436 nm (g-line)) is used to expose the film. The wafer is turned upside down on a carrier (a silicon wafer) and exposed through a mask (with circles of 20, 50 and 100 μm) with an exposure energy of $1750 \text{ mJ}/\text{cm}^2$. A proximity of 130 μm has been used.

Step 6: Post-exposure bake

A mobile hotplate is used to post-exposure bake the exposed film. The layer was baked immediately after exposure for 20 minutes at $95 \text{ }^\circ\text{C}$.

Step 7: Develop

Propylene glycol methyl ether acetate (PGMEA) is used to develop the microneedles by dissolving unexposed SU-8. The wafer was completely immersed in PGMEA by using a holder (Figure 5). The development has taken place with a spinning speed of 0 rpm for 100 minutes at cleanroom temperature.



Figure 5 — Developing SU-8

Step 8: Clean

Isopropyl alcohol (IPA) is used to clean the microneedles after development by spraying on it carefully. Subsequently, nitrogen is used to blow dry. Figure 6 shows the result of the process.

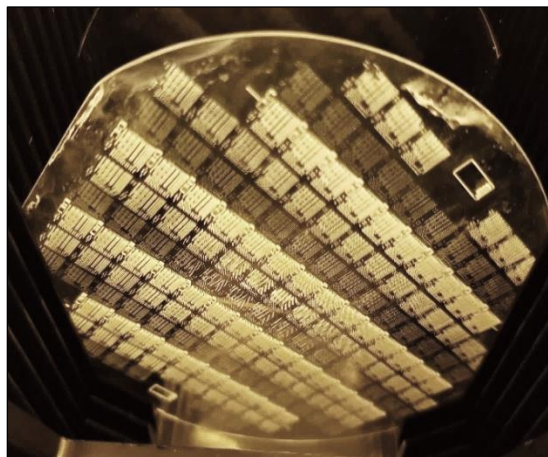


Figure 6 — Result of the process

5-3 Fabrication results

Prototype 1

Figure 7 shows that the microneedles of prototype 1 are bent. The smallest microneedles (the most left one) were bent the most. The stability of the microneedles is probably too low to withstand centrifugation (for drying). Another cause may be spinning during development.

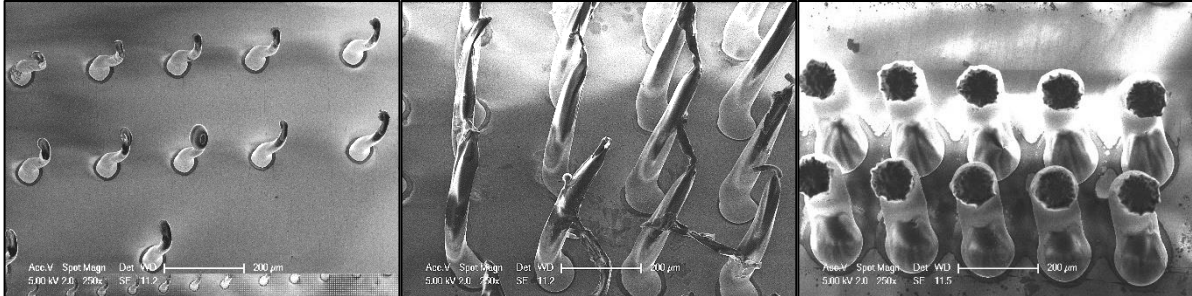


Figure 7 – Prototype 1 from left to right made with mask with circles with diameter of 20, 50 and 100 µm

Prototype 2

Centrifugation to dry the microneedles has been omitted in the process of creating prototype 2. However, the microneedles were still bent, in which the smallest microneedles were bent the most.

Prototype 3

Spinning during development has been omitted in the process of creating prototype 3. Figure 8 shows that microneedles are much more upright compared to the first two prototypes. The smallest microneedles are bent the most. After three prototypes it was clear that the microneedles resulting from the medium sized circles (50 µm) of the mask give the best results.



Figure 8 – Prototype 2 from left to right made with mask with circles with diameter of 20, 50 and 100 µm

Prototype 4

Compared to prototype 3, the exposure energy has been reduced with 750 mJ/cm² in this attempt. The goal was to obtain more tapered microneedles. Figure 9 shows a similar result as in attempt 3. However, the tip diameters of prototype 4 were slightly smaller.

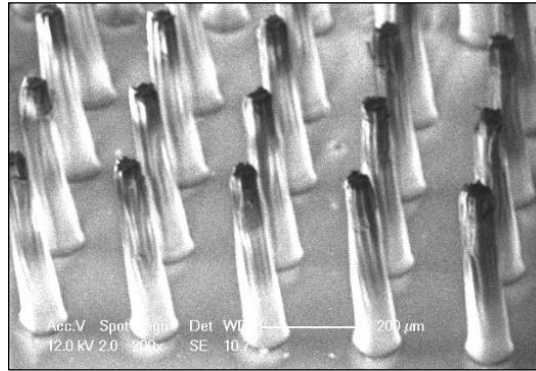


Figure 9 – Prototype 4

Prototype 5

Compared to prototype 4, the exposure energy has been reduced to 1000 mJ/cm² to create even more tapered microneedles. Figure 10 shows that this is the case, but that the surface also becomes rougher.



Figure 10 – Prototype 5

Prototype 6

Compared to prototype 5, the exposure energy has been reduced to 800 mJ/cm² to create even more tapered microneedles. Figure 11 shows that the microneedles are more tapered, but also bend more towards the tips. This is probably due to less stability.

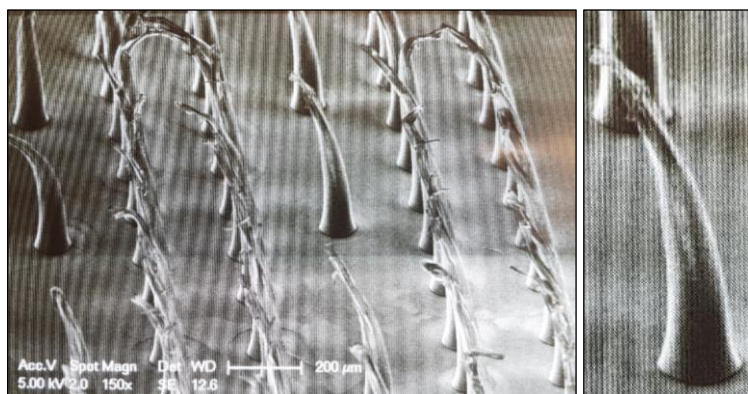


Figure 11 – Prototype 6

Prototype 7

Prototype 4 had the best result with the desired tip diameter. For this reason, prototype 7 looked at whether it is possible to create the film layer in one go instead of in two parts. Figure 12 shows that the microneedles are bent despite maintaining the same parameters as in prototype 4. Wrinkles appeared during the soft bake of the film. This usually indicates skin formation on the film. The bending probably has something to do with the amount of moisture in the layer that could no longer get out. Too much moisture in the microneedles can lead to less stability.

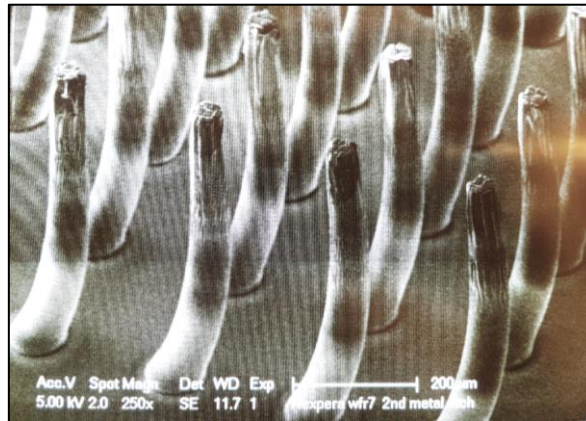


Figure 12 – Prototype 7

Prototype 8

To check whether the bending has anything to do with the soft baking, a longer baking time was used for this last prototype. This resulted also in skin forming during the soft bake and bending of the microneedles.

Conclusion

Prototype 4 has resulted in microneedles with the desired tip diameter. This means that, with a film thickness of 400 μm , a mask with circles of 50 μm and a proximity of 130 μm during exposure with an exposure energy of 1750 mJ/cm^2 , the desired microneedles in terms of dimensional aspects can be created.

6 Measurements

6-1 Dimensional aspects

The dimensional properties, i.e. the length, the base diameter and the tip diameter of the microneedles, have been determined using scanning electron microscopy (SEM). The microneedles from prototype 4 that were made with the mask circles with a diameter of 50 μm were measured with the SEM's built-in program at four places on the wafer. Table 1 shows the results.

	#1	#2	#2	#4	Mean
Length (μm)	420	417	405	398	410
Base diameter (μm)	101	110	108	105	106
Tip diameter (μm)	35	41	48	46	43

Table 1 – Dimensional properties of the microneedles

Conclusion

The microneedles have an average length of 410 μm , average base diameter of 106 μm and an average tip diameter of 43 μm .

6-2 Mechanical failure

The FT-NMT04 Nanomechanical Testing System (FemtoTools) has been used to quantify the fracture point of the microneedles when pressing onto it vertically (at the tip) and horizontally (at the base). A nanoindenter with a tip diameter of 20 μm is used to deliver the force. To make sure that the nanoindenter was in full contact with the microneedle, calibration was performed to obtain an accurate position of the nanoindenter relative to the microneedle using an optical microscope on the system.

Multiple vertical compression tests have been performed. When pushing on the tip (Figure 1), the microneedle starts bending (Figure 2), first showing elastic behaviour and then changing to plastic behaviour, and finally breaks. Two of the vertical compression tests were meaningful. Figure 4 shows the result of the first vertical compression test. This shows that the microneedle breaks at a force of 78.1 mN and a displacement of 63 μm . The ultimate strength is 88.6 mN. Figure 5 shows the results of the second vertical compression test. This shows that the microneedle breaks at a force of 67.0 mN and a displacement of 62 μm . The ultimate strength is 96.7 mN.

There was no movement in the horizontal compression test at the base with the maximum force of the testing system (Figure 3). The force required for this is therefore higher than the maximum force of the testing system, which is equal to 200 mN.

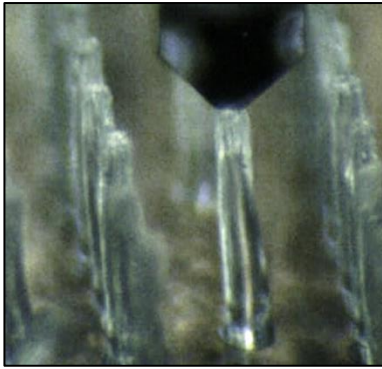


Figure 1 – Vertical compression

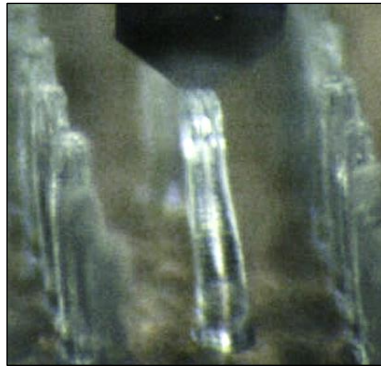


Figure 2 – Microneedle bends backwards

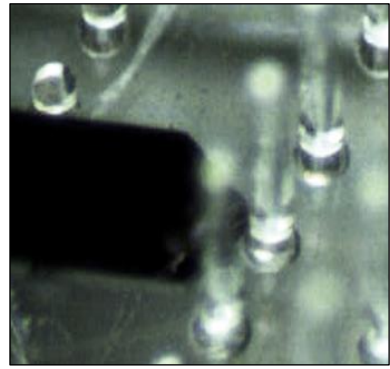


Figure 3 – Horizontal compression

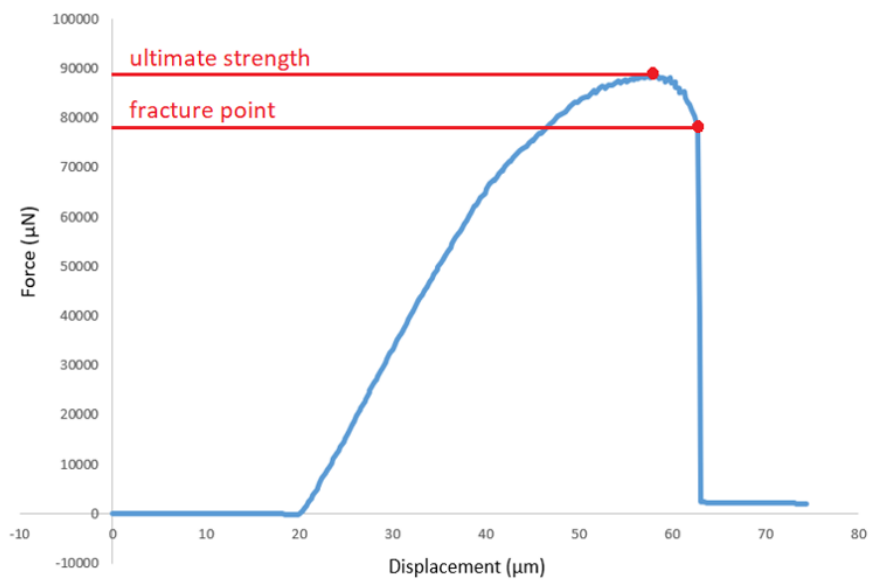


Figure 4 – Vertical compression test 1 of one microneedle

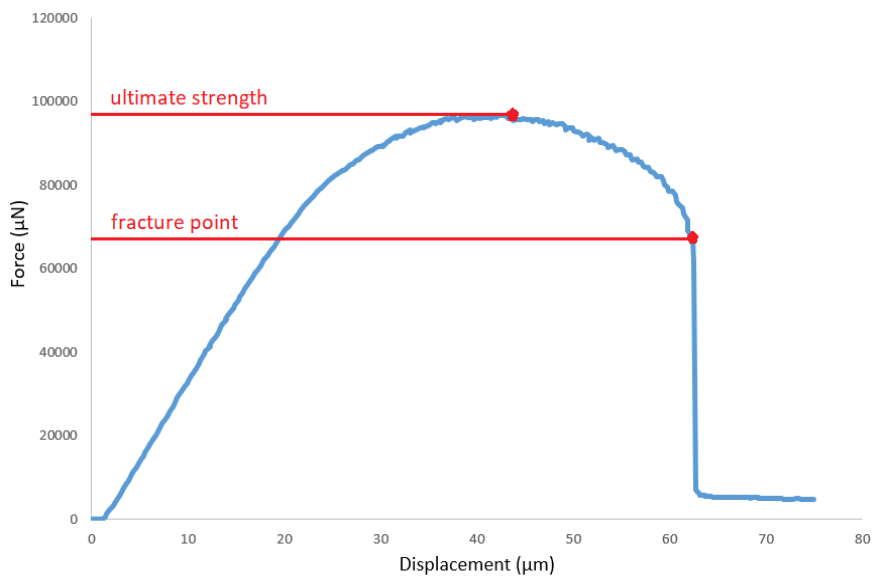


Figure 5 – Vertical compression test 2 of one microneedle

Conclusion

With a vertical compression test on the tip of the microneedle, the average fracture point of one microneedle is at a force of 72.5 mN and an average displacement of 63 μm . The average fracture force per area microneedle is therefore is 16.5 N/mm^2 . However, the number of necessary microneedles still needs to be investigated. The use of more microneedles will influence the fracture point.

6-3 Transmission

The transmission of the microneedles is measured to quantify the maximum amount of light that can be passed through the microneedles from the base and from the tip, and the difference between them (loss of light). However, in vivo there is no transmission.

The transmission of the microneedles is measured from both the base and the tip, since the microneedles will be used to both send light into the skin and receive light from the skin. Figure 6 shows the measurement setup. A microscope, the Flame Miniature Spectrometer (Ocean Optics), the SPLIT400-UV-VIS fiber (Ocean Optics) and the software 'Ocean View' (Ocean Optics) were used for this. The fiber consists of three fibers, two fibers on one end and a third fiber on the other end (Figure 7A). The core diameter of each fiber is 200 μm , and the wavelength range is 300 – 1100 nm.

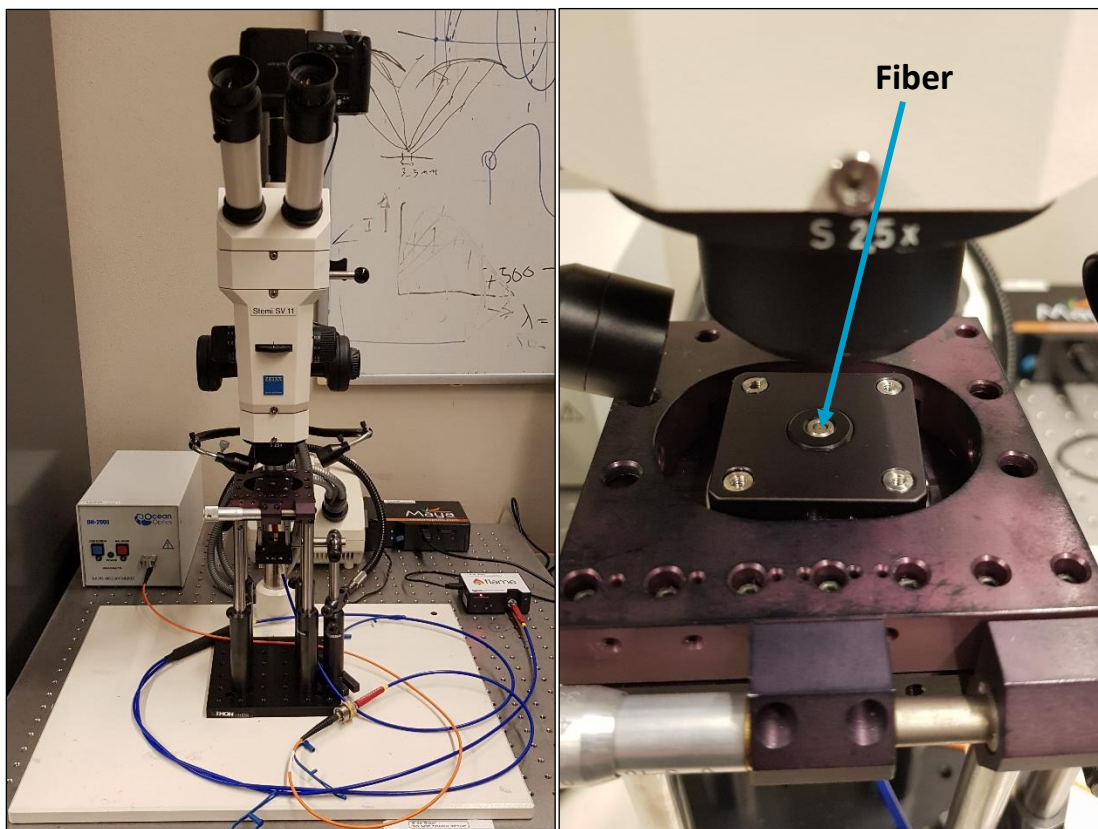


Figure 6 - Measurement setup

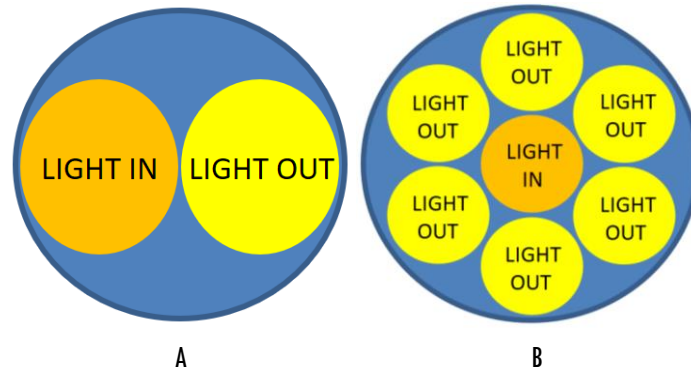


Figure 7 – Fibers (A: SPLIT400-UV-VIS, B: FCR-7UV200)

The transmission was measured from the base. The light from the microscope has been used as a source. First, the transmission from the light source is calibrated to a transmission of 100 %. Then, the transmission through the substrate with the microneedles was measured, which turned out to be 86 %. This transmission loss is caused by reflection from the fiber (glass) to air, from air to the substrate (glass) and from the substrate to the microneedles (SU-8). The first transition, from the fiber to air, has a difference of 0.5 (1.5 – 1.0) in refractive index. The resulting reflection can be calculated as follows:

$$R = \left| \frac{n_1 - n_2}{n_1 + n_2} \right|^2 = \left| \frac{1.5 - 1.0}{1.5 + 1.0} \right|^2 = 0.04$$

Thus, the transition from the fiber to air leads to 4 % of reflection. The second transition, from air to the substrate (glass) equals the reflection during the first transition and is therefore 4 %. The third transition, from the substrate to the microneedles, has a difference of –0.2 (1.5 – 1.7) in refractive index. This leads to 0.4 % of reflection. Therefore, there is 91.6 % light left. This is the theoretical value, but with the measurements this value turned out to be 86 %. To reduce the reflection at the substrate, optical glue or an anti-reflective coating on the substrate can be used to eliminate the reflection between the fiber and the substrate.

To measure the extent to which the microneedles transmit light from the tip, skin simulations are made from gelatin (gelatin granules mixed with water, 20 % by weight), and to measure whether the microneedles pass the correct wavelength, blue food colorant has been added (Figure 8).



Figure 8 – Gelatin for transmission measurements

For the transmission measurements through the microneedles, the microneedles are pressed into the gelatin. Because the spaces between the microneedles are not covered, the light also passes through these spaces (Figure 9). As a result, optical measurements will not be accurate, because these spaces participate. To eliminate these spaces as much as possible, gelatin has been covered on one side with a permanent black marker, so that the light that meets these spaces is absorbed (Figure 10). In Figure 9 and 10, absorption and scattering are not considered; it only shows schematically what the difference is between covering and not covering the spaces between the microneedles.

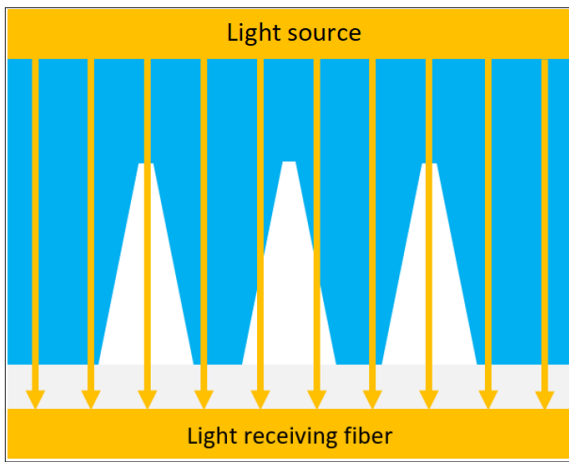


Figure 9 – Non-covered transmission from tip to base

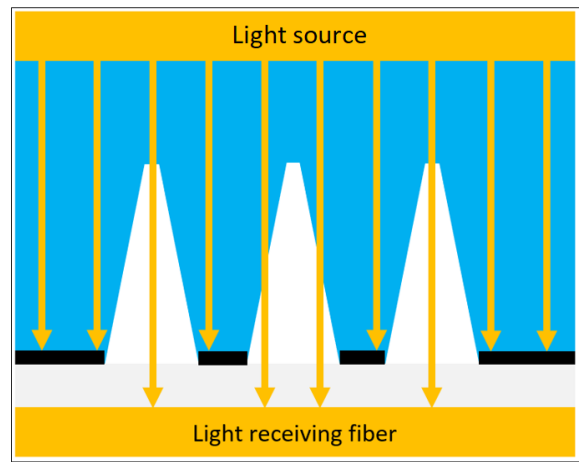


Figure 10 – Covered transmission from tip to base

Figure 11 and Table 2 show the results of the transmission measurements from the base of the microneedles. Transmission from the base to the tip of the microneedles give a reduction of 14 % caused by the substrate with the microneedles. When the microneedles are punctured in blue colored gelatin, peaks in the blue spectrum can be observed. This results in a reduction in transmission of 24 %. Covering the spaces between the microneedles gives a reduction in transmission of 70 %. Covering the spaces between the microneedles results in a clear difference. The microneedles alone therefore have a transmission of 30 % from the base.

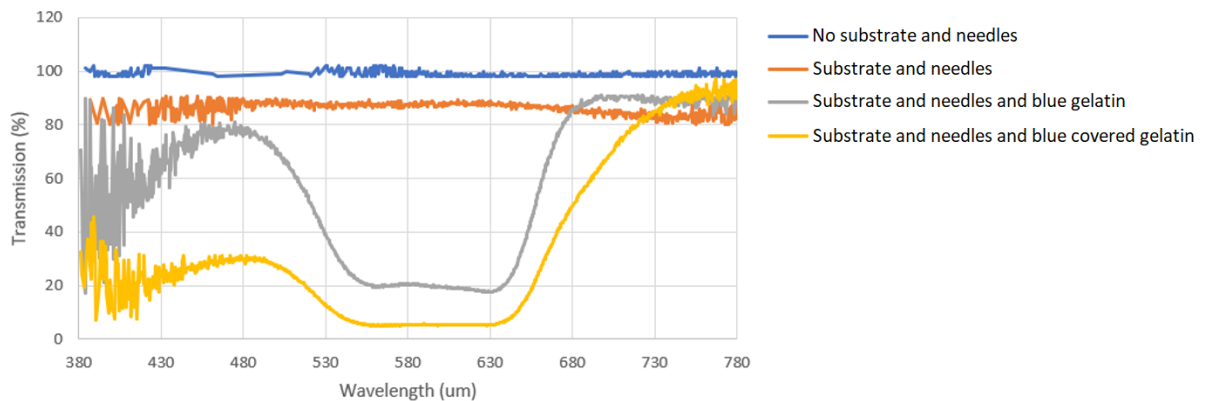


Figure 11 – Transmission from the base in blue gelatin

	Wavelength (nm)	Transmission (%)
Substrate with needles	-	86
Substrate with needles and blue gelatin	476 - 495	76
Substrate with needles and blue covered gelatin	476 - 495	30

Table 2 – Results of transmission measurements from the base

The same measurements are performed from the tip of the microneedles. Figure 12 and Table 3 show the results. Transmission measurements from the tip to the base of the microneedles give a reduction of 14 % caused by the substrate and the microneedles, same as with transmission from the base. When the microneedles are punctured in blue colored gelatin, peaks in the blue spectrum can be observed. This results in a reduction in transmission of 39 %. Covering the spaces between the microneedles gives a reduction in transmission of 75 %. Thus, the transmission from the tip to the base is lower compared to the transmission from the base to the tip. This is because the tip of the microneedles has a smaller diameter compared to its base.

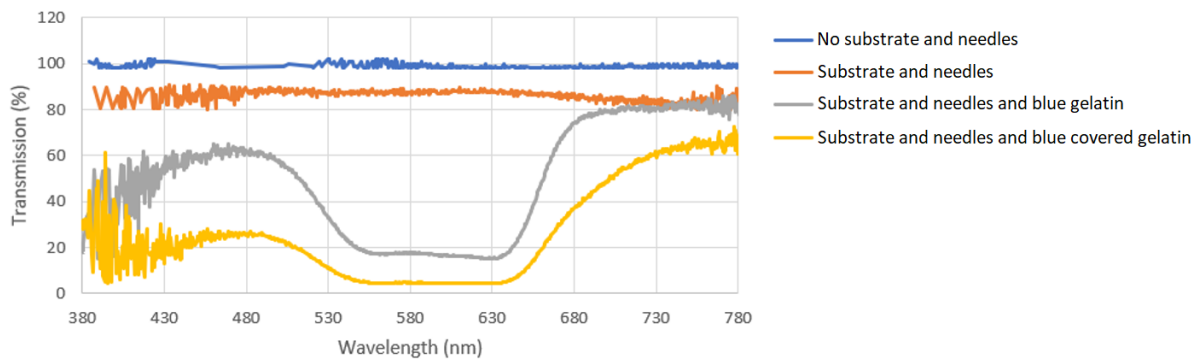


Figure 12 – Transmission from the tip in blue gelatin

	Wavelength (nm)	Transmission (%)
Substrate with needles	-	86
Substrate with needles and blue gelatin	476 - 495	61
Substrate with needles and blue covered gelatin	476 - 495	25

Table 3 – Results of transmission measurements from the tip

Conclusion

There is a lot of light loss through the microneedles; 70 % with the transmission from the base and 75 % with the transmission from the tip. The transmission reduction by the microneedles where the spaces between the microneedles are covered is comparable for measurements from the base (61 %) and the tip (59 %). The maximum amount of light that can pass through the tip of the microneedles to the sensor is 25 %. However, because the light is already reduced by 70 % if it propagates from the base to the tip, the maximum amount of light that can propagate back from the tip to the base is 7.5 %. This amount can therefore be used for reflection measurements.

6-4 Reflection

The amount of bilirubin can be measured by taking reflection measurements. Therefore, it has been tested if the microneedles are functioning for reflection measurements. Real skin contains scattering and absorbent particles. For this reason, a skin simulation was made from water (15 g), gelatin (5 g) and semi-skimmed milk (10 g) with yellow, blue, green and red dye (Figure 13). Semi-skimmed milk contains approximately 35 % casein micelles, an animal protein, with a diameter ranging between 50 and 250 nm [50]. Different dye concentrations have been used to simulate differences in bilirubin concentrations.

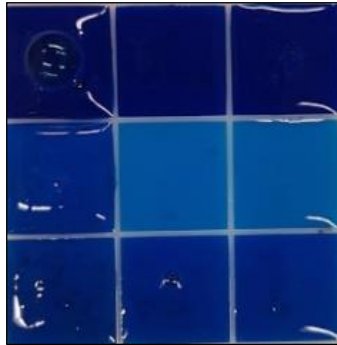


Figure 13 — Skin simulation (blue) for reflection measurements

The measurement setup of the reflection measurements is comparable to the measurement setup of the transmission measurements (Figure 6). However, the DH-2000 UV-VIS-NIR (Ocean Optics) is used as light source, and instead of the SPLIT400-UV-VIS fiber, the FCR-7UV200 fiber (Ocean Optics) is used, because no meaningful results could be obtained with the SPLIT400-UV-VIS. The FCR-7UV200 fiber consists of seven fibers, one central fiber to bring in light with six surrounding fibers to capture reflected light (Figure 7B). The core diameter of each fiber is 200 μm , and the wavelength range is 200 – 800 nm.

The reflection is measured from the base, as it would be with a measurement in the clinical setting. First, the system is calibrated to a reflection of 0 %. Then, the reflection was measured with only the substrate with the microneedles. This has resulted in 10 % of reflection, slightly lower than with the transmission measurements. The microneedles were also used in these measurements without covering and covering the spaces in between.

Yellow gelatin is interesting to simulate reflection measurements with bilirubin, because bilirubin is yellow, and therefore absorbs in the blue spectrum (peak of bilirubin is 460 nm). This is because the color that is absorbed by a pigment is the complementary color (green line) of that pigment, and blue is the complementary color of yellow. The reflection measurements in yellow gelatin show the expected spectrum (Figure 14). There is a dip in the curves for the wavelengths of blue, in other words, there is absorption in the blue spectrum. In addition, a difference in the height of the curve can be seen between light and dark yellow. The results with the microneedles where the spaces are covered are the most representative. With these measurements, dark yellow shows less reflection at 460 nm, this is due to more absorption due to the presence of more yellow pigments in dark yellow. The reflection in light yellow and in dark yellow at 460 nm is 32 and 14 % respectively. Logically,

differences in reflections can also be seen in the yellow spectrum; dark yellow shows less reflection compared to light yellow, because there is more absorption by dark yellow.

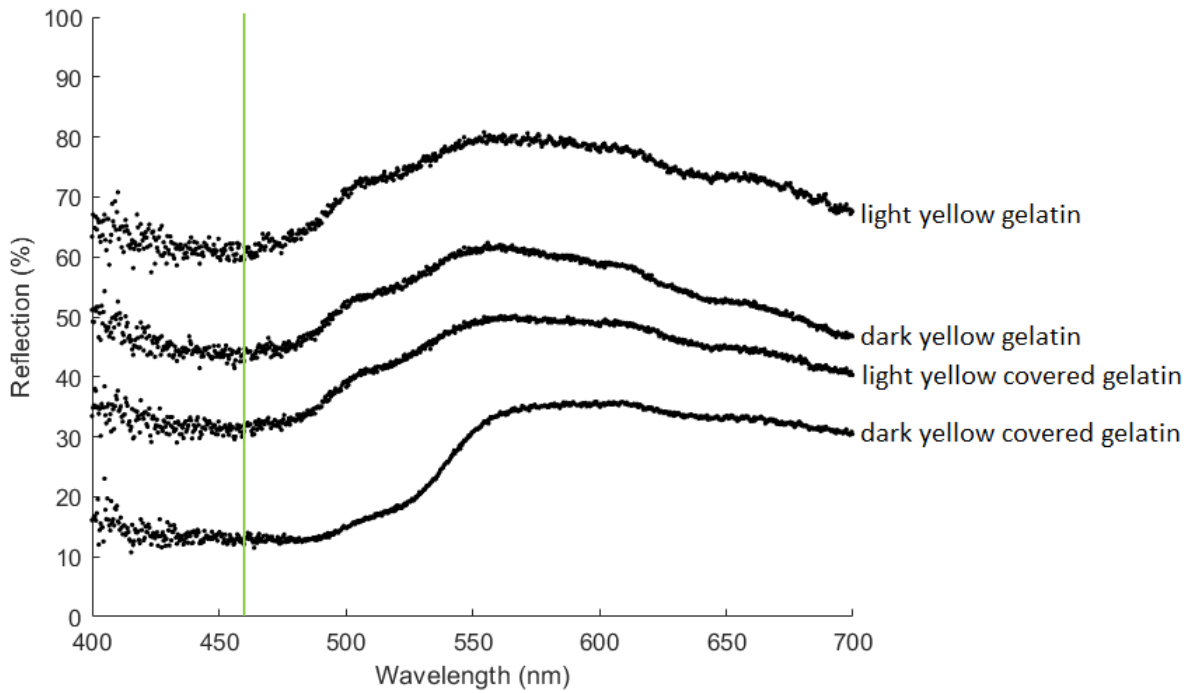


Figure 14 – Reflection in yellow gelatin

To show that the microneedles also show the expected results for other colors, the measurements were also carried out in blue (Figure 15) and red gelatin (Figure 16).

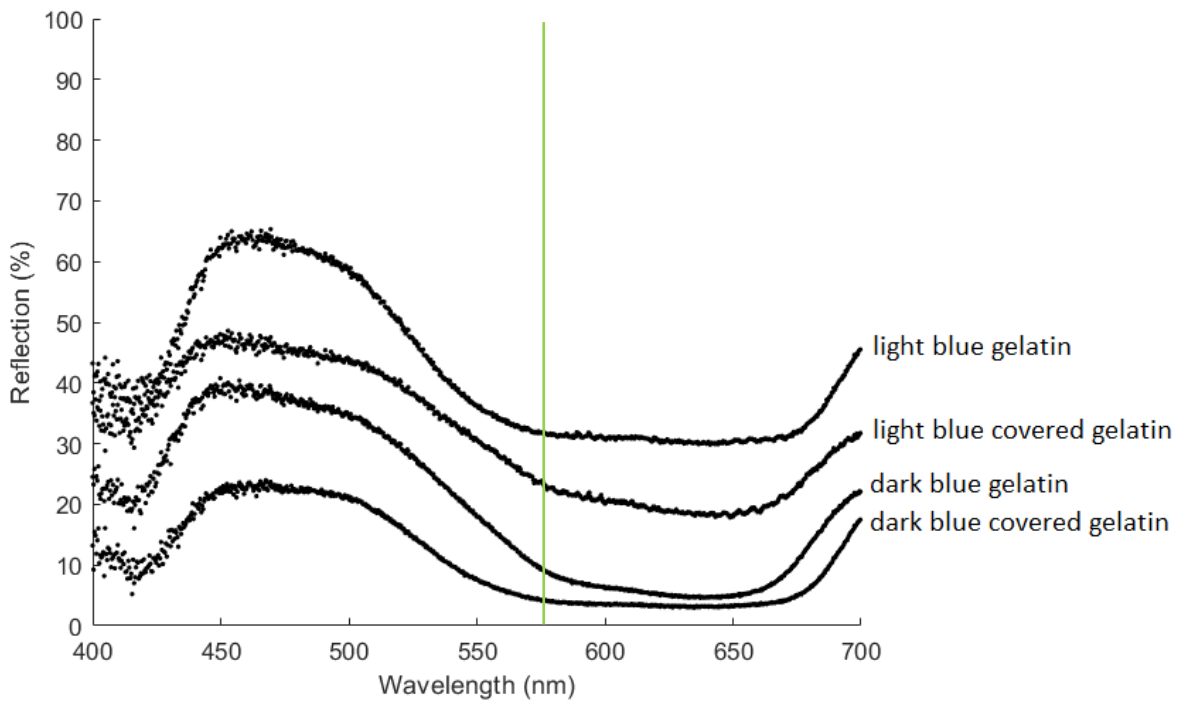


Figure 15 – Reflection in blue gelatin

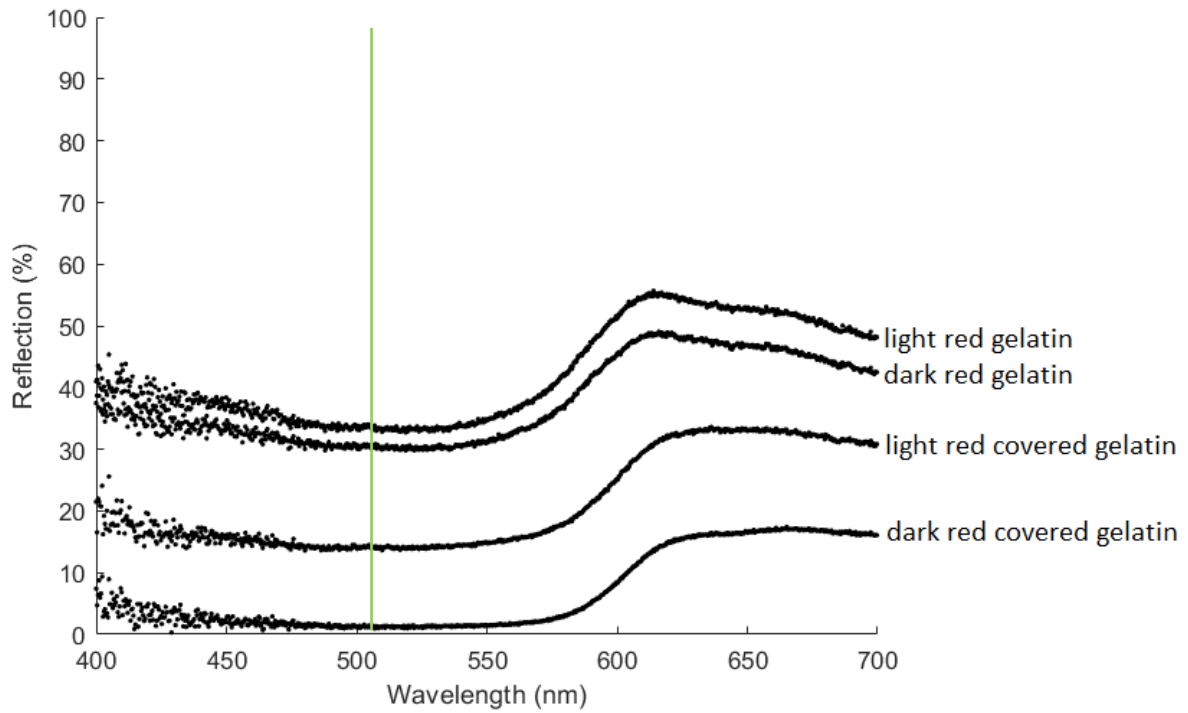


Figure 16 – Reflection in red gelatin

Figure 15 shows, as expected, a peak in the blue spectrum. In Figure 16 this applies to the red spectrum. Both figures also show that a dark variant of the gelatin shows less reflection, because more absorption occurs due to more pigment use. The complementary colors (green lines) of blue and red are yellow (± 575 nm) and cyan (± 505 nm) respectively. The results of the measurements with covered gelatin are summarized in Table 4.

	Wavelength peak (nm)	Reflection (%)	Difference (%)
Light yellow	575	50	
Dark yellow	575	35	-15
Light blue	470	48	
Dark blue	470	24	-24
Light red	680	32	
Dark red	680	17	-15

Table 4 – Results of reflection measurements with covered gelatin

Conclusion

The measurements with the microneedles where the spaces are covered results in all measurements in lower reflection values compared to the microneedles where these spaces are not covered. The differences in color concentrations also result in differences in reflection values. The dark variants of the colors show less reflection in all measurements. This is caused by a higher absorption. Also, as expected, the measurements in simulated bilirubin (yellow gelatin) show a dip in the blue spectrum, e.g. at 460 nm, the absorption peak of bilirubin. Thus, measuring reflection using microneedles as a 'tunnel' seems possible.

7 Conclusion and future work

The aim of this project was to develop microneedles for optical spectroscopy, and to test them in simulated skin to determine the usability for reflection measurements.

The microneedles for this purpose had to meet several conditions. The microneedles had to be biocompatible, able to puncture the skin, enough mechanical strength for insertion into the skin, minimally invasive, and optically transparent for the wavelengths of bilirubin. Therefore, the polymer SU-8 has been chosen, because this material is biocompatible and optically transparent for the desired wavelengths. Furthermore, based on literature research it was determined that the length of the microneedle should be a maximum of 480 μm to keep it minimally invasive and the tip diameter should be around 40 μm to allow enough light to pass through, but also to be sharp enough to puncture the skin easily. The microneedles have been developed by using microfabrication techniques with a focus on backside exposure. Multiple prototypes have been developed and evaluated based on dimensional properties. The prototype closest to the requirements was chosen to take measurements. These were the microneedles with an average length of 410 μm , an average base diameter of 106 μm and an average tip diameter of 43 μm . These microneedles were developed with a film thickness of 400 μm , a mask with circles of 50 μm and a proximity of 130 μm during exposure with an exposure energy of 1750 mJ/cm^2 . Although this method has resulted in the desired microneedles, it is recommended to investigate other, perhaps easier, methodologies, for example, micromoulding or 3D-printing, in which, for example, uniformity of the microneedles can be optimized. Furthermore, research must be conducted into optimization in the manufacturing process to cover the spaces between the microneedles.

The mechanical properties of the skin play a role in puncturing the skin. When puncturing the skin, the needle will experience resistive forces exerted by the skin. In order to puncture the skin, the ultimate stress of the skin must be overcome by pushing perpendicular to the skin with the needle to bend and stretch the skin. Therefore, the mechanical failure point of the microneedles was investigated with an indentation test on the tip of an individual microneedle. The tests showed that the average fracture point of one microneedle is at a force of 72.5 mN and an average displacement of 63 μm . The average fracture point per area microneedle is 16.5 N/mm^2 . According to the literature, the theoretical force required to puncture the skin is 3.2 N/mm^2 . The average fracture point per area microneedle is higher compared to the skin, so with an insertion force between 3.2 and 16.5 N/mm^2 , it is possible to puncture the skin with one microneedle. An application device to push the microneedles into the skin can be used to limit the mechanical failure of the microneedles, in this way, the microneedle does not have to be manually pushed into the skin and variations in insertion angle, and therefore the unwanted forces on the microneedles (i.e. shear stress), are minimized. In addition, the required number of microneedles for bilirubin measurements still needs to be investigated. The use of more microneedles will influence the fracture force. It is further recommended to use a different method for investigating the mechanical properties of the microneedles, since the method used in this project was limited to nanosized objects.

To determine if the microneedles can be used for reflection measurements, transmission and reflection measurements were performed on simulated skin made from gelatin. The transmission measurements have shown that the maximum amount of light that can pass through the tip of the microneedles to the sensor is 25 %. However, because the light is already reduced by 70 % if it propagates from the base to the tip, the maximum amount of light that can propagate back from the tip to the base is 7.5 %. This amount can therefore be used for reflection measurements. The reflection measurements have shown that measuring reflection using microneedles as a 'tunnel' seems possible. The differences in color concentrations in the simulated skin results in differences in reflection values. The dark variants show less reflection in all measurements. This is caused by a higher absorption due to the higher amount of pigment use. Also, as expected, the measurements in simulated bilirubin (skin simulation with yellow colorant) show a dip in the blue spectrum, e.g. at 460 nm, the absorption peak of bilirubin. However, despite the good initial results of these measurements, perhaps more signal is needed to accurately measure significant concentration differences. In the measurements of this project, an attenuator is used that is set randomly. In the ideal situation, the signal should be as large as possible as long as it is safe for use in the skin. In addition, research can be done into other designs of the microneedles, in which possibly more efficient use can be made of light. A possible design that can be investigated is the use of a 'mirror' in the tip of the microneedles.

In addition to the requirements that have been met in this project, there are more requirements that the entire device must meet. Firstly, the microneedles must be easy to integrate with the spectrometer. The spectrometer will be reconnected to the (disposable) microneedles for each patient, so the alignment between these components must be reliable. In future research, the optimal alignment between the microneedles and the optical spectrometer must be investigated. In addition, research must be done in how the microneedles can be used as disposable microneedles. Besides that, the device must also be operable by people without qualifications, since there is little to no qualified staff in remote African areas. Therefore, research into the easiest possible operation of the system must be done. Furthermore, the use of the device must be accurate and reliable in clinical application. First, research can be done with real bilirubin. If the measurements are accurate and the entire system is complete, research can be done on living test subjects with different skin colors, possibly also in remote African areas. Moreover, the device must be cheap to produce, since it is for remote African areas, so research needs to be done into mass production opportunities and costs. Lastly, this project was focused on the detection of bilirubin in blood using a minimally invasive system, although there may be many more applications for the fabricated microneedles. For example, in future research it could be investigated whether this device can be applied to glucose measurements in diabetic patients.

In short, in this project microneedles have been developed that are minimally invasive, biocompatible, optically transparent, and easy-to-process. The first measurements have shown that it seems possible to use the microneedles in combination with optical spectroscopy to detect differences in "bilirubin" concentrations. Moreover, the microneedles can be used to puncture the skin without fracturing. In this project the focus was on concretizing a possible solution. Therefore, there is still plenty of future research to do to optimize and ultimately implement this device.

References

1. Brits, H., Adendorff, J., Huisamen, D., Beukes, D., Botha, K., Herbst, H., & Joubert, G. (2018). The prevalence of neonatal jaundice and risk factors in healthy term neonates at National District Hospital in Bloemfontein. *African Journal of Primary Health Care and Family Medicine* 10(1), 1-6.
2. Veenstra, C., Petersen, W., Vellekoop, I. M., Steenbergen, W., & Bosschaart, N. (2018). Spatially confined quantification of bilirubin concentrations by spectroscopic visible-light optical coherence tomography. *Biomedical Optical Express* 9(8), 3581-3589.
3. Olusanya, B. O., Osibanjo, F. B., Mabogunje, C. A., Slusher, T. M., & Olowe, S. A. (2016). The burden and management of neonatal jaundice in Nigeria: A scoping review of the literature. *Nigerian Journal of Clinical Practice* 19(1), 1-17.
4. Bhutani, V. K., Zipursky, A., Blencowe, H., Khanna, R., Sgro, M., & Ebbesen, F. (2013). Neonatal hyperbilirubinemia and Rhesus disease of the newborn: incidence and impairment estimates for 2010 at regional and global levels. *Pediatric Research* 74, 86-100.
5. Medex Supply (2019). Respiroics BiliChek Noninvasive Bilirubin Meter. Consulted on 12-11-2019 via: https://www.medexsupply.com/nicu-and-infant-care-jaundice-management-jaundice-tests-respiroics-bilichek-noninvasive-bilirubin-meter-wall-mount-power-supply-x_pid-48903.html
6. Olusanya, B. O., Imosemi, D. O., & Emokpae, A. A. (2016). Differences between transcutaneous and serum bilirubin measurements in black African neonates. *Pediatrics* 138(3), e20160907.
7. Wilson, B. C., Jermyn, M., & Leblond, F. (2019). Challenges and opportunities in clinical translation of biomedical optical spectroscopy and imaging. *Journal of Biomedical Optics* 23(3), 030901.
8. Kwon, K. Y., Khomenko, A., Haq, M., & Li, W. (2013). Integrated Slanted Microneedle-LED Array for Optogenetics. *35th Annual International Conference of the IEEE EMBS*, 249-252.
9. Rejinold, N. S., Shin, J., Yong Seok, H., & Kim, Y. (2015). Biomedical applications of microneedles in therapeutics: recent advancements and implications in drug delivery. *Expert Opinion on Drug Delivery* 13(1), 109-131.
10. Joodaki, H., & Panzar, M. B. (2018). Skin mechanical properties and modeling: A review. *Journal of Engineering in Medicine* 232(4), 1-21.
11. Agarwal, S., & Krishnamurthy, K. (2019). Skin histology. Treasure Island: StatPearls Publishing.
12. Dongre, A. (2016). 3. X-ray Interactions. In Singh, H., Sasane, A., & Lodha, R. (Eds.), *Textbook of Radiology Physics (pp. 12-15)*. New Delhi, India: Jaypee Brothers Medical Publishers.
13. Salomatina, E., Jiang, B., Novak, J., & Yaroslavsky, A. N. (2006). Optical properties of normal and cancerous human skin in the visible and near-infrared spectral range. *Journal of Biomedical Optics* 11(6), 064026.
14. Baranoski, G. V. G. & Chen, F. T. (2017). Optical Properties of Skin Surface. In: Humbert, P., Fanian, F., Maibach, H. I., & Agache, P. (Eds.). *Agache's Measuring the Skin (pp. 85-98)*. Cham, Switzerland: Springer.
15. Alla, S. K., Clark, J. F., & Bayette, F. R. (2009). Signal processing system to extract serum bilirubin concentration from diffuse reflectance spectrum of human skin. *IEEE Engineering in Medicine and Biology Society*, 1290-1293.

16. Javid, B., Fotouhi-Ghazvini, F., & Zakeri, F. S. (2018). Noninvasive optical diagnostic techniques for mobile blood glucose and bilirubin monitoring. *Journal of Medical Signals and Sensors* 8(3), 125-139.
17. Lodha, R., Deorari, A. K., Jatana, V., & Paul, V. K. (2000). Non-invasive estimation of total serum bilirubin by multi-wavelength spectral reflectance in neonates. *Indian Pediatrics* 37(7), 771-775.
18. Mohamad, M., & Manap, H. (2015). The optimal absorption of bilirubin using an optical fibre sensor. *Journal of Engineering and Applied Sciences* 10(19), 8762-8764.
19. Sudha, G. F., Senthil Kumaran, G., Thirumorthi, J., Balamurugan, K., & Anand, M. (2007). Optical monitoring of bilirubin-simulation and experimental results. *Journal of Optics* 36(2), 87-97.
20. Veenstra, C., Petersen, W., Vellekoop, I. M., Steenbergen, W., & Bosschaart, N. (2018). Spatially confined quantification of bilirubin concentrations by spectroscopic visible-light optical coherence tomography. *Biomedical Optical Express* 9(8), 3581-3589.
21. Dolci, A., & Panteghini, M. (2014). Harmonization of automated hemolysis index assessment and use: Is it possible? *Clinica Chimica Acta* 432, 38-43.
22. Lilien, L. D., Harris, V. J., Ramamurthy, R.S., & Pildes, R. S. (1976). Neonatal osteomyelitis of the calcaneus: complication of heel puncture. *The Journal of Pediatrics* 88, 478-480.
23. Jacquemond, C., Bruyere-Garnier, K., & Coret, M. (2007). Methodology to determine failure characteristics of planar soft tissues using a dynamic tensile test. *Journal of Biomechanics* 40(2), 468-475.
24. Joodaki, H., & Panzer, M. B. (2018). Skin mechanical properties and modeling: A review. *Journal of Engineering in Medicine* 232(4), 323-343.
25. Aggarwal, P., & Johnston, C. R. (2004). Geometrical effects in mechanical characterizing of microneedle for biomedical applications. *Sensors and Actuators B* 102, 226-234.
26. Philips N.V. (2019). Mother & Child Care: Jaundice management. Consulted on 12-11-2019 via: <https://www.philips.nl/healthcare/product/HC989805644871/bilichek-bilirubinometer>
27. Swarna, S., Pasupathy, S., Chinnasami, B., Manasa, N., & Ramraj, B. (2017). The smart phone study: assessing the reliability and accuracy of neonatal jaundice measurement using smart phone application. *International Journal of Contemporary Pediatrics* 5(2), 285-289.
28. Taylor, J. A., Stout, J. W., De Greef, L., Goel, M., Patel, S., Chung, E. K., Koduri, A., McMahon, S., Dickerson, J., Simpson, E. A., & Larson, E. C. (2017). Use of a smartphone app to assess neonatal jaundice. *Pediatrics* 140(3), e20170312.
29. Aydın, M., Hardalaç, F., Ural, B., & Karap, S. (2016). Neonatal jaundice detection system. *Journal of Medical Systems* 40(7), 166.
30. Munkholm, S. B., Krogholt, T., Ebbesen, F., Szecsi, P. B., & Kristensen, S. R. (2018). The smartphone camera as a potential method for transcutaneous bilirubin measurement. *PLoS One* 13(6), e0197938.
31. Chandra, A., Seshadri, N. P. G., & Periyasamy, R. (2017). Skin reflectometry technique for measurement of bilirubin concentration to detect jaundice. *ACM International Conference Proceeding Series Part F131935*, 22-26.
32. Ong, P. E., Huong, A. K. C., Hafizah, W. M., Tay, K. G., & Philimon, S. P. (2016). Reflectance spectroscopy system for noninvasive prediction of skin bilirubin concentration related parameter. *Biomedical Engineering and Sciences* 7843472, 352-355.
33. Babity, S., Roohnikan, M., & Brambilla, D. (2019). Advances in the design of transdermal microneedles for diagnostic and monitoring applications. *Small* 14(49), 1803186.

34. Barrett, C., Dawson, K., O'Mahony, C., & O'Riordan, A. (2015). Development of low cost rapid fabrication of sharp polymer microneedles for in vivo glucose biosensing applications. *Journal of Solid State Science and Technology* 4(1), 3053-3058.
35. Hwa, K., Subramani, B., Chang, P., Chien, M., & Huang, J. (2015). Transdermal microneedle array-based sensor for real time continuous glucose monitoring. *International Journal of Electrochemical Science* 10(3), 2455-2466.
36. Kim, K. B., Lee, W., Cho, C., Park, D., Cho, S. J., & Shim, Y. (2019). Continuous glucose monitoring using a microneedle array sensor coupled with a wireless signal transmitter. *Sensors and Actuators B: Chemical* 281, 14-21.
37. Bollella, P., Sharma, S., Cass, A. E. G., & Antiochia, R. (2019). Microneedle-based biosensor for minimally-invasive lactate detection. *Biosensors and Bioelectronics* 123, 152-159.
38. Yoon, H. S., Lee, S. J., & Park, J. Y. (2014). A non-enzymatic micro-needle patch sensor for free-cholesterol continuous monitoring. *Proceedings of IEEE Sensors* 6985005, 347-350.
39. Mirza, K. B., Zuliani, C., Hou, B., Siong Ng, F., Peters, N. S., & Toumazou, C. (2017). Injection moulded microneedle sensor for real-time wireless pH monitoring. *Engineering in Medicine and Biology Society* 8036794, 189-192.
40. Miller, P. R., Narayan, R. J., & Polsky, R. (2016). Microneedle-based sensors for medical diagnosis. *Journal of Materials Chemistry B* 4(8), 1379-1383.
41. Ciui, B., Martin, A., Mishra, R. K., Brunetti, B., Nakagawa, T., Dawkins, T. J., Lyu, M., Cristea, C., Sandulescu, R., & Wang, J. (2018). Wearable wireless tyrosinase bandage and microneedle sensors: Toward melanoma screening. *Advanced Healthcare Materials* 7(7).
42. Mohan, A. M. V., Windmiller, J. R., Mishra, R. K., & Wang, J. (2017). Continuous minimally-invasive alcohol monitoring using microneedle sensor arrays. *Biosensors and Bioelectronics* 91, 574-579.
43. Miller, P. R., Narayan, R. J., & Polsky, R. (2016). Microneedle-based sensors for medical diagnosis. *Journal of Materials Chemistry B* 4(8), 1379-1383.
44. Ventrelli, L., Strambini, L. M., & Barillaro, G. (2015). Microneedles for transdermal biosensing: current picture and future direction. *Advanced Healthcare Materials* 4, 2606-2614.
45. Gill, H. S., Denson, D. D., Burris, B. A., & Prausnitz, M. R. (2008). Effect of microneedle design on pain in human subjects. *The Clinical Journal of Pain* 24(7), 585-594.
46. MicroChem. SU-8 2000: Permanent epoxy negative photoresist. Processing guidelines for: SU-8 2025, SU-8 2035, SU-8 2050 and SU-8 2075.
47. Singh, T. R. R., Mcmillan, H., Mooney, K., Alkilani, A. Z., & Donnelly, R. F. (2013). Microneedles for drug delivery and monitoring. In Li, X. J., & Zhou, Y. (Eds.), *Microfluidic Devices for Biomedical Applications* (pp. 185-230). Cambridge, UK: Woodhead Publishing Series.
48. Kim, Y. C., Park, J. H., & Prausnitz, M. R. (2012). Microneedles for drug and vaccine delivery. *Advanced Drug Delivery Reviews* 64(14), 1547-1568.
49. Liqun, D. U., Zhongzhou, W., Xiaopeng, R., Shengli, C., & Qing, S. (2015). Fabrication of SU-8 microneedle based on backside exposure technology. *Key Engineering Materials* 645-646, 853-858.
50. Michalski, M., Briard, V., & Michel, F. (2001). Optical parameters of milk fat globules for laser light scattering measurements. *Le Lait* 81(6), 787-796.

A1. Flowchart for 'microneedle'

(grey = glass, blue = SU-8, red = mask)

1. Preparing

1. Pour ± 30 ml SU-8 2075 from original bottle in a cup
2. Store cup on cleanroom temperature at least 2 hours before use

2. Spin-coating and soft-baking

1. Spin-coating a layer of 200 μm of SU-8 2075, poured from a cup
 - Amount: ± 10 ml
 - Recipe:
 1. Spin speed: 500 rpm, acceleration: 100 rpm/second, spin time: 5 seconds
 2. Spin speed: 1300 rpm, acceleration: 300 rpm/second, spin time: 30 seconds
2. Rest for 5 minutes
3. Edge bead removal with a swab soaked in acetone
4. Soft bake at 65 °C for 10 minutes and at 95 °C for 60 minutes
5. Cool for 10 minutes at cleanroom temperature

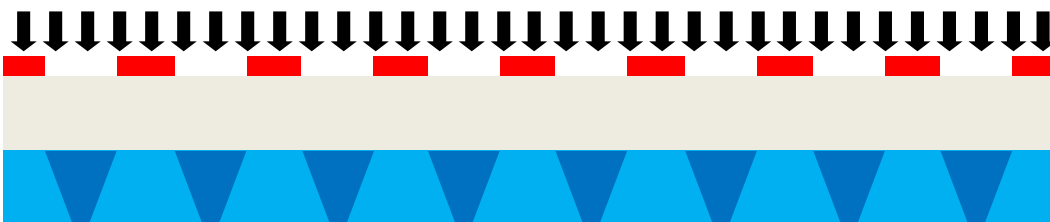


3. Repeat step 1 to create a second film layer



4. Alignment and exposure

1. Placing mask (mask with circles with a diameter of 50 μm)
2. Backside exposing with a dose of 1750 mJ/cm^2 with a proximity of 130 μm



5. Post-exposure baking and developing

1. Post-exposure baking on hotplate at 95 °C for 20 minutes
2. Developing by immersion in PGMEA for 100 minutes at 0 rpm and cleanroom temperature



6. Cleaning

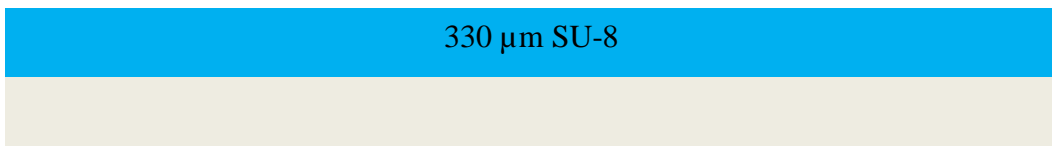
1. Cleaning with isopropyl alcohol by spraying
2. Blow dry with nitrogen

A2. Flowchart for 'microneedle with convex mirror'

Note: The following is just a concept of processing steps that can be taken to develop microneedles with a convex mirror (grey = glass, blue = SU-8, orange = metal layer, green = photoresist, red = mask).

1. Spin-coating

1. Spin-coating a layer of 110 μm of SU-8 2075, dispensed by a pump
 - Amount: ± 7 ml
 - Recipe:
 1. Spin speed: 500 rpm, acceleration: 100 rpm/second, spin time: 10 seconds
 2. Spin speed: 2000 rpm, acceleration: 300 rpm/second, spin time: 30 seconds
2. Edge bead removal with a swab
3. Soft bake at 65 °C for 5 minutes and at 95 °C for 20 minutes



2. Repeat step 1 to create the second layer

3. Repeat step 2 to create the third layer

4. Exposure

1. Frontside exposing with a dose of 700 mJ/cm^2



5. Developing

1. Post-exposure bake at 95 °C for 25 minutes



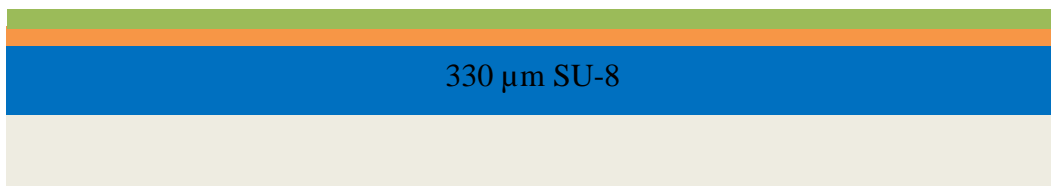
6. Metallization

1. Sputter coat 200 nm Al (100% Al)
 - Recipe: Temperature: 350 °C, Ar flow: 100 sccm
2. Visual inspection: the metal layer must look shiny



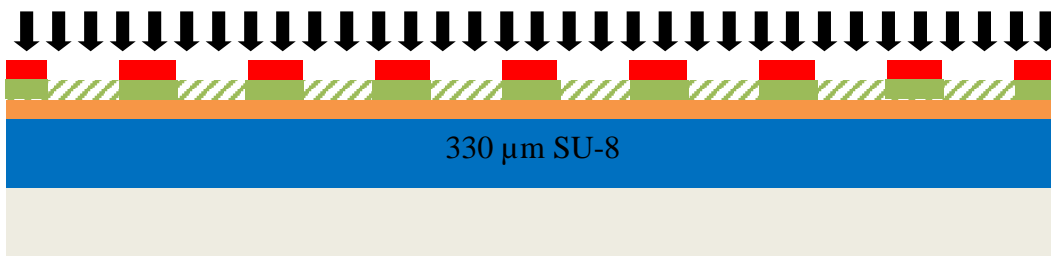
7. Coating with photoresist

1. Check relative humidity ($48 \pm 2\%$) in the room before coating
2. Use program positive resist
 - Treatment with HMDS (hexamethyldisilazane) vapor, with nitrogen as a carrier gas
 - Spin-coating of positive resist, dispensed by a pump
 - Soft bake at 95 °C for 90 seconds
 - Automatic edge bead removal with a solvent



8. Alignment and exposure

1. Placing mask
2. Frontside exposing with a dose of 500 mJ/cm^2



9. Developing

1. Use program "1-Dev – SP"
 - Post-exposure bake at 115 °C for 90 seconds
 - Developing with developing material
 - Hard bake at 100 °C for 90 seconds



10. Wet etching Al

1. Etching in H_3PO_4 solution at 85 °C for 1 minute



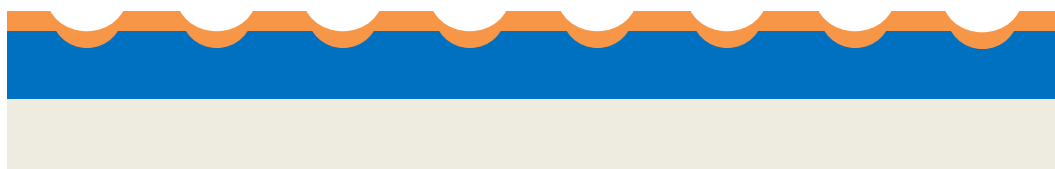
11. Plasma etching

1. Recipe:
 - Step: bulk etch (RIE)
 - Gasses: CF_4 and O_2 in 1 : 20
 - RF power: 100 w
 - Etch time: 5 minutes
 - He pressure: ?
 - Chamber pressure: 20 mbar



12. Metallization

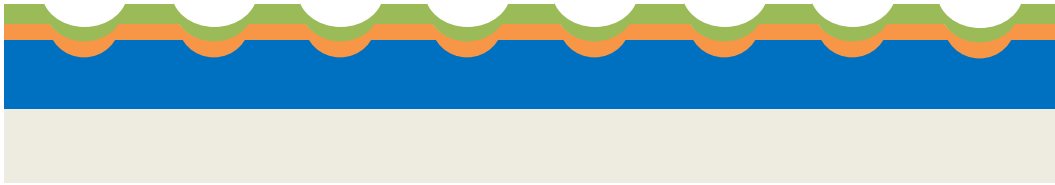
1. Sputter coat 200 nm Al (100% Al)
 - Recipe: Temperature: 350 °C, Ar flow: 100 sccm
2. Visual inspection: the metal layer must look shiny



13. Coating with photoresist

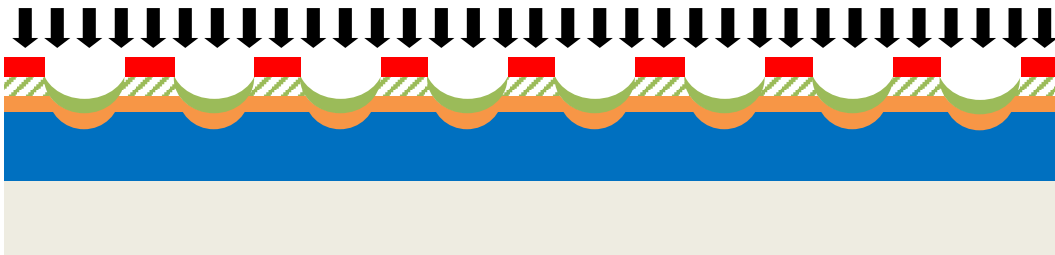
1. Check relative humidity ($48 \pm 2\%$) in the room before coating
2. Use program for negative resist
 - Treatment with HMDS (hexamethyldisilazane) vapor, with nitrogen as a carrier gas
 - Spin-coating of resist, dispensed by a pump

- Soft bake at 95 °C for 90 seconds
- Automatic edge bead removal with a solvent



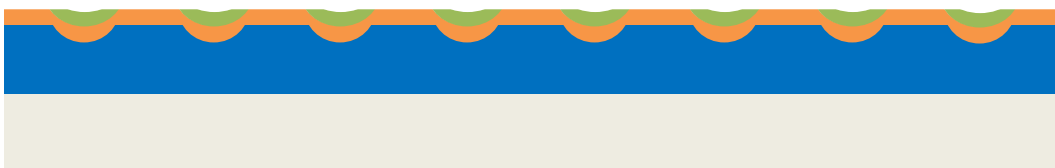
14. Alignment and exposure

1. Placing mask [existing mask with circles]
2. Frontside exposing with a dose of 500 mJ/cm²



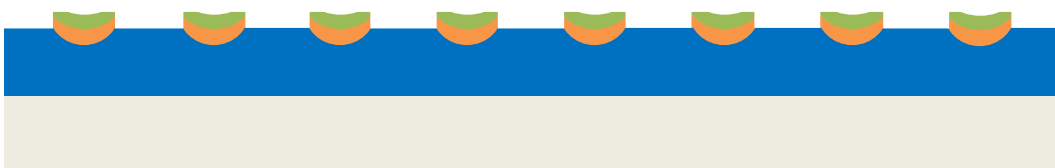
15. Developing

1. Use program "1-Dev – SP"
 - Post-exposure bake at 115 °C for 90 seconds
 - Developing with developing material
 - Hard bake at 100 °C for 90 seconds



16. Wet etching Al

1. Etching in H₃PO₄ solution at 85 °C for 1 minute



17. Plasma etching

1. Recipe:
 - Step: bulk etch (RIE)
 - Gasses: CF_4 and O_2 in 1 : 20
 - RF power: 100 w
 - Etch time: 5 minutes
 - He pressure: ?
 - Chamber pressure: 20 mbar



18. Spin-coating

1. Treatment with HMDS (hexamethyldisilazane) vapor, with nitrogen as a carrier gas
2. Spin-coating a layer of $60 \mu\text{m}$ of SU-8 2075, dispensed by a pump
 - Amount: $\pm 7 \text{ ml}$
 - Recipe:
 1. Spin speed: 500 rpm, acceleration: 100 rpm/second, spin time: 10 seconds
 2. Spin speed: 4000 rpm, acceleration: 300 rpm/second, spin time: 30 seconds
3. Edge bead removal with a swab
4. Soft bake at $65 \text{ }^\circ\text{C}$ for 3 minutes and at $95 \text{ }^\circ\text{C}$ for 9 minutes



19. Exposure

1. Frontside exposing with a dose of 1000 mJ/cm^2



20. Developing

1. Post-exposure bake at 95 °C for 5 minutes



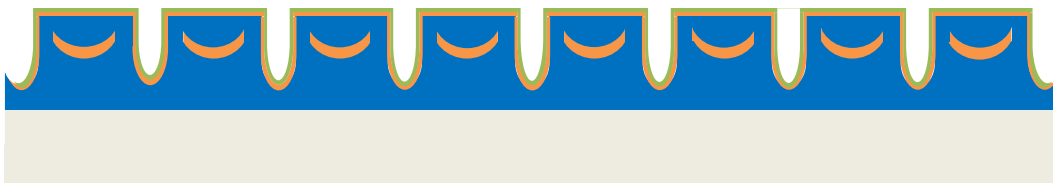
21. Metallization

1. Sputter coat 200 nm Al (100% Al)
 - Recipe: Temperature: 350 °C, Ar flow: 100 sccm
2. Visual inspection: the metal layer must look shiny



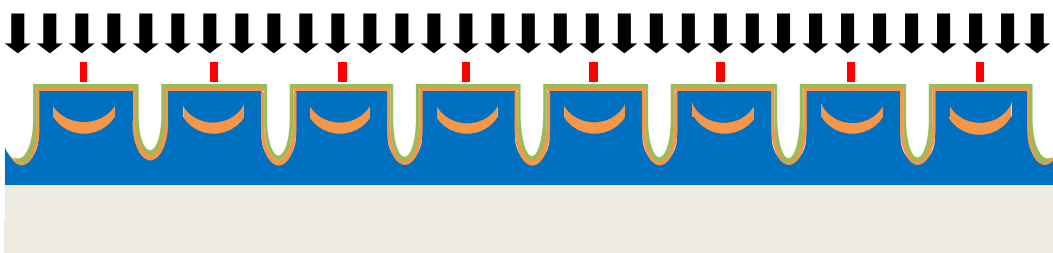
22. Coating with photoresist

1. Check relative humidity ($48 \pm 2\%$) in the room before coating
2. Use program for positive resist
 - Treatment with HMDS (hexamethyldisilazane) vapor, with nitrogen as a carrier gas
 - Spin-coating of positive resist, dispensed by a pump
 - Soft bake at 95 °C for 90 seconds
 - Automatic edge bead removal with a solvent



23. Alignment and exposure

1. Placing mask [mask with tiny circles]
2. Frontside exposing with a dose of 1000 mJ/cm²



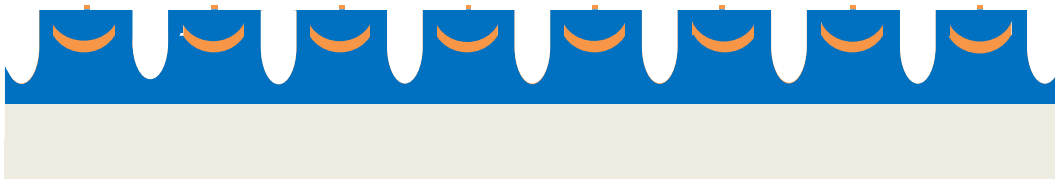
24. Developing

1. Use program "1-Dev – SP"
 - Post-exposure bake at 115 °C for 90 seconds
 - Developing with developing material
 - Hard bake at 100 °C for 90 seconds



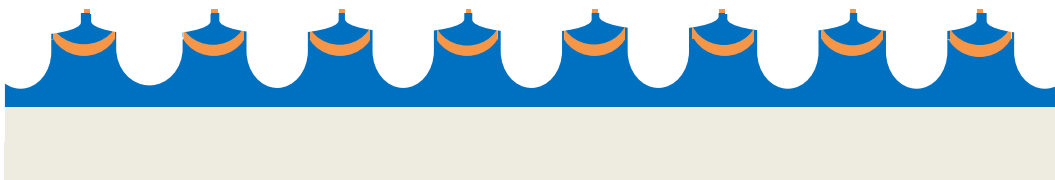
25. Wet etching Al

1. Etching in H_3PO_4 solution at 85 °C for 1



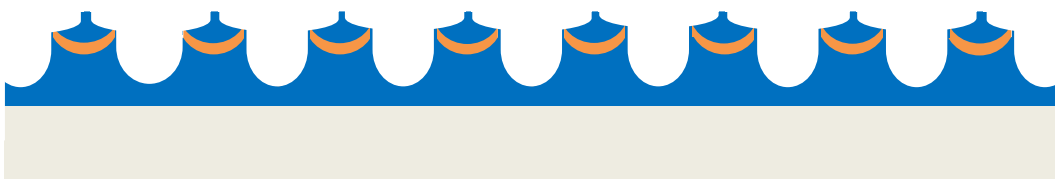
26. Plasma etching

1. Recipe:
 - Step: bulk etch (RIE)
 - Gasses: CF_4 and O_2 in 1 : 20
 - RF power: 100 w
 - Etch time: 5 minutes
 - He pressure: ?
 - Chamber pressure: 20 mbar



27. Layer stripping

1. Strip Al layer with H_3PO_4 solution



28. Cleaning

1. Cleaning with isopropyl alcohol and deionized water
2. Air dry